Click Here for Full Article

# Characterizing polar atmospheres and their effect on Rayleigh-scattering optical depth

Claudio Tomasi,[1] Boyan Petkov,[1,2] Robert S. Stone,[3,4] Elena Benedetti,[5] Vito Vitale,[1] Angelo Lupi,[1] Mauro Mazzola,[1] Christian Lanconelli,[1] Andreas Herber,[6] and Wolfgang von Hoyningen-Huene[7]

[1] A large set of radiosoundings was analyzed to study the dependence of Rayleigh-scattering optical depth (ROD) on pressure and temperature features of the polar clear-sky atmosphere. This set consists of 1320 radiosoundings, launched throughout the year at six Arctic sites, and of 940 radiosoundings launched at five Antarctic sites. The vertical profiles of pressure, temperature, and relative humidity given by these radiosoundings were corrected for lag errors and dry biases and then completed up to 120 km altitude, using COSPAR International Reference Atmosphere (CIRA) monthly vertical profiles of pressure and temperature, water vapor mixing ratio data derived from various satellite observations, and standard $CO_2$ vertical profile relative to 2007, when the ground-level concentration was 380 ppmv. Calculations of the volume Rayleigh-scattering coefficient were made for all the radiosoundings to study its seasonal variations with height due to pressure and temperature changes occurring in the troposphere and stratosphere. It was found that the surface-level pressure and temperature conditions can account to a large extent for these seasonal effects. Therefore, average spectral evaluations of ROD were made at 88 selected wavelengths from 0.20 to 4.0 $\mu$m for all the radiosoundings, subdivided into eight latitude/altitude site classes, representing 70°N, 75°N, 80°N, 70°S, 75°S, 80°S, and 90°S latitudes, for which the average ground values of air pressure $p_a$ and air temperature $T_a$ were defined. The dependence of ROD on the daily ground-level values of air pressure $p_o$ and air temperature $T_o$ measured at each site can be accounted for by using an algorithm in which the pressure dependence is given with good approximation by ratio $(p_o/p_a)$, and the temperature linear dependence is expressed by the difference $(T_a - T_o)$ multiplied by a spectral slope coefficient $k(\lambda)$ which varies by site classification. This algorithm was estimated to provide values of ROD with accuracy within ±0.5% at the six sea-level Arctic sites, ±0.5% at the three Antarctic coastal sites, and ±0.7% at the two Antarctic Plateau sites (Dome C and South Pole). When used to analyze the Sun photometer measurements, the present evaluations of ROD are estimated to provide aerosol optical depth values at visible wavelengths with relative errors of 1%–2% at the Arctic sites, 1%–4% at the coastal Antarctic sites, and 3%–13% at the Antarctic Plateau sites, for background aerosol extinction conditions.

[1] Institute of Atmospheric Sciences and Climate, Consiglio Nazionale delle Ricerche, Bologna, Italy.
[2] International Centre for Theoretical Physics, Trieste, Italy.
[3] Cooperative Institute for Research in Environmental Sciences, University of Colorado, Boulder, Colorado, USA.
[4] Earth System Research Laboratory, NOAA, Boulder, Colorado, USA.
[5] ICES Group, Institute of Acoustic "O.M. Corbino," Consiglio Nazionale delle Ricerche, Rome, Italy.
[6] Climate System Division, Alfred Wegener Institute for Polar and Marine Research, Bremerhaven, Germany.
[7] Remote Sensing, Institute of Environmental Physics, University of Bremen, Bremen, Germany.

## 1. Introduction

[2] Surface-level aerosol mass concentration is, in general, very low in the polar regions for clean air conditions, with monthly mean values smaller than 10 $\mu$g m$^{-3}$ at Arctic sites [*Quinn et al.*, 2002; *Ström et al.*, 2003], equal to a few $\mu$g m$^{-3}$ at the Antarctic coastal sites [*Minikin et al.*, 1998; *Teinilä et al.*, 2000], and appreciably lower than 1 $\mu$g m$^{-3}$ at the high-altitude sites on the Antarctic Plateau [*Bodhaine*, 1996; *Piel et al.*, 2006]. In both regions, the aerosol particles sampled at coastal sites were found to consist mainly of small marine particles, of high concentration, and, to a lesser extent, sea salt particles and mineral dust. Along the Antarctic coasts,

the coarse particle modes were found to contribute moderately to the overall mass concentration, which includes negligible contents of soot particles [*Shaw*, 1988; *Wolff and Cachier*, 1998; *Quinn et al.*, 2002; *Ström et al.*, 2003; *Sharma et al.*, 2006]. Conversely, the aerosols sampled at the Antarctic Plateau sites consist mainly of fine non-sea-salt (nss) sulfate particles, originated through subsidence processes from the free troposphere that are usually associated with long-range transport from the oceanic regions [*Hogan et al.*, 1979; *Bigg*, 1980; *de Mora et al.*, 1997].

[3] Correspondingly, very low background values of aerosol optical depth (AOD) at visible wavelengths are generally measured at the polar sites [*Shaw*, 1982; *Stone*, 2002], producing relatively weak features of incoming direct solar irradiance attenuation. Multispectral Sun photometer measurements performed at the Arctic stations of Barrow (Alaska), Alert (Nunavut, Canada), Summit (Greenland), Ny Ålesund (Svalbard), ALOMAR (Norway), Sodankilä (Finland), Vaida Bay (Barents Sea), Severnaya Zemlya (Siberia), Dikson Island (Siberia), and Kotel'ny Island (Siberia) were found to yield average daily values of AOD(500 nm) in the range 0.03–0.10 during summer months, for background conditions of atmospheric turbidity [*Radionov et al.*, 1994; *Herber et al.*, 1996, 2002; *Nagel et al.*, 1998; *Stone*, 2002; *Myhre et al.*, 2006; *Toledano et al.*, 2006; *Aaltonen et al.*, 2006; *Tomasi et al.*, 2007], giving values of the *Ångström* [1964] exponent $\alpha$ varying in general between 0.5 and 2.0 [*Vitale and Radionov*, 2005; *Tomasi et al.*, 2007]. In Antarctica, at the coastal and low-altitude sites of Terra Nova Bay, Neumayer, Mirny, Syowa, and Aboa, the daily mean values of AOD(500 nm) were found to vary between 0.01 and 0.06 [*Tomasi et al.*, 1989, 1991; *Vitale and Tomasi*, 1990; *Herber et al.*, 1993; *Radionov*, 1994; *Radionov et al.*, 1994, 2002; *Cacciari et al.*, 2000; *Virkkula et al.*, 2000; *Di Carmine et al.*, 2005], with values of $\alpha$ in the range 0.40–1.80. Lower values of AOD(500 nm) were determined at the high-altitude sites of Kohnen, Dome C, and South Pole [*Stone*, 2002; *Six et al.*, 2005], varying most frequently between 0.005 and 0.03, with values of $\alpha$ generally higher than 1.2 and sometimes exceeding 2.0 in cases where the aerosol loading consists predominantly of small-size nss sulfate particles.

[4] Thus, molecular scattering is the dominant mechanism leading to atmospheric extinction of solar radiation in the cloudless polar atmosphere. That is, Rayleigh-scattering optical depth (ROD) is usually greater than AOD at visible and near-infrared (IR) wavelengths at high latitudes for clean background conditions. This is the case in the absence of Arctic haze [*Shaw*, 1983; *Bodhaine and Dutton*, 1993], boreal smoke from forest fires [*Forster et al.*, 2001; *Damoah et al.*, 2004; *Stohl et al.*, 2006], and Asian dust [*Stone et al.*, 2005] that is transported from low latitudes, or incursions of volcanic aerosols at stratospheric levels [*Dutton and Christy*, 1992; *Stone et al.*, 1993; *Herber et al.*, 1996]. Reliable calculations of ROD have been performed at several wavelengths, from the ultraviolet (UV) to the near-IR, in the recent years, (1) using realistic physical models to describe the interactions of incoming radiation with air molecules along the atmospheric vertical path [*Bucholtz*, 1995; *Bodhaine et al.*, 1999; *Tomasi et al.*, 2005], and (2) for the U.S. standard atmosphere model and the supplementary standard atmosphere models defined

for different seasons and latitudes [*Anderson et al.*, 1986]. Among these supplementary models, the subarctic summer (July, 60°N) model represents the most similar conditions to those taking place at Arctic sites in the summer months, giving values of ROD which decrease by more than 2 orders of magnitude, from 1.212 to 0.0086, as the wavelength increases from 0.30 to 1.00 $\mu$m [*Tomasi et al.*, 2005]. Such a model provides values of ROD, which are considerably greater than those of AOD measured at Arctic sites, throughout the UV and visible spectral range, and comparable with those of AOD at the near-IR wavelengths, for clean air atmospheric conditions.

[5] The calculations of the spectral values of sea-level volume Rayleigh-scattering coefficient $\beta(\lambda, 0)$ at wavelength $\lambda$, made by *Tomasi et al.* [2005] for the six standard atmosphere models, indicate that this parameter varies appreciably as a function of temperature. In fact, it decreases by about 9% at 45°N latitude, as the surface temperature $T_o$ increases from 272.2 to 294.2 K, and by 12% at 60°N latitude, as $T_o$ increases from 257.2 to 287.2 K. These evaluations indicate that ROD should vary appreciably throughout the year also at the Arctic and Antarctic sites, where the atmospheric temperature is subject to significant seasonal changes.

[6] Following the Sun photometry method, the values of total atmospheric optical depth are obtained from Sun photometer measurements of direct solar irradiance by applying the Lambert-Beer law [*Shaw*, 1976] to each monochromatic signal measured at the surface. The values of AOD are then calculated at each wavelength as the difference between the total atmospheric optical depth and the sum of the optical depth contributions due to gaseous absorption (water vapor, ozone, nitrogen dioxide, and oxygen dimer) and Rayleigh-scattering (ROD). Considering that the spectral values of ROD are in general considerably greater than those of AOD for clean air conditions of the polar atmospheres, a relatively small error in determining ROD can lead to a larger error in evaluating AOD at all visible and near-IR wavelengths.

[7] Given this level of uncertainty, a detailed analysis of the sensitivity of ROD to variations in atmospheric structure is warranted. Values of ROD were computed using the algorithm of *Tomasi et al.* [2005] for realistic vertical profiles of air pressure, temperature, and moisture measured at Arctic and Antarctic sites during the annual cycle. These calculations are presented here at wavelengths ranging from 0.20 to 4.00 $\mu$m, for their use in the analysis of multispectral Sun photometer measurements and evaluation of AOD, examination of the ground-based measurements of UV solar radiation [*Petkov et al.*, 2006], retrieval of AOD from satellite data [*von Hoyningen-Huene et al.*, 2003], and more generally for studying the radiative transfer processes occurring in the polar atmosphere [*Tanaka et al.*, 1986; *Solomon et al.*, 1987; *Larsen et al.*, 1994].

## 2. Dependence of the Volume Rayleigh-Scattering Coefficient on Wavelength and Meteorological Parameters

[8] A composite algorithm was determined by *Tomasi et al.* [2005] to evaluate the effects exerted on the Rayleigh-scattering coefficient by (1) moist air refractive index and its
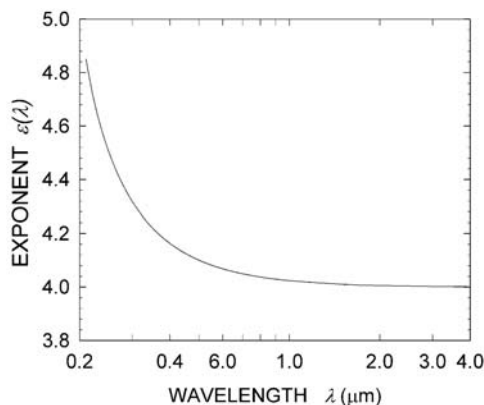
**Figure 1.** Spectral dependence curve of the Rayleigh-scattering exponent $\varepsilon(\lambda)$ in equation (1), with the slope coefficient gradually decreasing from 4.8509 to 4.0015 throughout the $0.21-3.9$ $\mu$m wavelength range.

dependence on wavelength, air pressure, temperature, water vapor partial pressure, and $CO_2$ volume concentration and (2) depolarization, represented in terms of the King factor, which depends on the molecular concentrations of the main gaseous constituents of air ($N_2$, $O_2$, Ar, and $CO_2$) and water vapor partial pressure. Using this algorithm, it is possible to obtain realistic evaluations of the monochromatic volume Rayleigh-scattering coefficient $\beta(\lambda, z)$ at the various heights, from which calculations of Rayleigh-scattering optical depth ROD$(\lambda)$ are obtained at each wavelength $\lambda$ by integrating $\beta(\lambda, z)$ along the vertical path of the atmosphere, from the sea level to the top-of-the-atmosphere (TOA) level $z_\infty$ which here is assumed to be 120 km, as in standard atmosphere models [*Anderson et al.*, 1986]. These aspects are examined in this section.

## 2.1. Dependence of the Volume Rayleigh-Scattering Coefficient on Wavelength

[9] Coefficient $\beta(\lambda, z)$ gives the measure of total molecular scattering in cloudless air at height $z$. It is calculated as the product of the molecular number density $N(z)$ of air at height $z$ by the total Rayleigh-scattering cross section $\sigma(\lambda, z)$ per molecule, where (1) $N(z)$ varies as a function of total air pressure $p(z)$ and air temperature $T(z)$ and (2) $\sigma(\lambda, z)$ is evaluated according to the classical equation adopted by *Bodhaine et al.* [1999] for incident unpolarized (natural) radiation, expressed as a function of monochromatic refractive index $n(\lambda, z)$ of moist air, monochromatic King factor $F(\lambda, z)$ for the depolarization of air, and number density $N(z)$.

[10] In the algorithm proposed by *Tomasi et al.* [2005], the refractive index $n(\lambda, z)$ is calculated as a function of wavelength, air pressure, temperature, water vapor partial pressure $e(z)$, and $CO_2$ volume concentration $C(z)$, all of which vary as a function of height according to results achieved from both theoretical and experimental studies on air refractive index [*Dalgarno and Kingston*, 1960; *Edlén*, 1966; *Owens*, 1967; *Peck and Reeder*, 1972; *Bideau-Mehu et al.*, 1973]. The details of the improved algorithm proposed by *Ciddor* [1996, 2002], to account for the refractivity effects due to dry air containing $CO_2$ and water vapor, are carefully described by *Tomasi et al.* [2005], who used also a new formula of the *King* [1923] depolarization factor

$F(\lambda, z)$ based on a five-term equation in place of that most commonly available in the literature [*Young*, 1980; *Bates*, 1984]. It was deemed more accurate than those used previously because it describes more realistically the effects due to the dry air constituents (nitrogen, oxygen, and argon) and includes also two additional terms related to the atmospheric contents of $CO_2$ and water vapor.

[11] As mentioned above, the volume Rayleigh-scattering coefficient $\beta(\lambda, z)$ depends at each level $z$ on wavelength $\lambda$, because it is proportional to the cross section $\sigma(\lambda, z)$ through a factor equal to $N(z)$, and $\sigma(\lambda, z)$ is a function of moist air refractive index $n(\lambda, z)$ and King factor $F(\lambda, z)$, both varying with wavelength. Calculations of $\beta(\lambda, z)$ were made at some wavelengths ranging from 0.2 to 4.0 $\mu$m, at the sea level of a polar atmosphere, presenting total air pressure $p_o = 980$ hPa, temperature $T_o = 270$ K, and relative humidity (RH)$_o$ = 40%. The results obtained at the various wavelengths indicate that $\beta(\lambda, z)$ decreases gradually as wavelength increases, according to the inverse power of wavelength defined by the Rayleigh-scattering theory [*Penndorf*, 1957; *Bucholtz*, 1995; *Bodhaine et al.*, 1999] as follows:

$$\beta(\lambda, z) = \beta(z)\lambda^{-\varepsilon(\lambda)}, \tag{1}$$

where exponent $\varepsilon(\lambda)$ assumes values gradually decreasing from 4.8509 to 4.0015 throughout the $0.21-3.9$ $\mu$m wavelength range, as can be seen in Figure 1.

## 2.2. Dependence of the Volume Rayleigh-Scattering Coefficient on Air Pressure, Temperature, and Moisture Parameters

[12] Parameter $\beta(\lambda, z)$ depends on both total air pressure $p(z)$ and air temperature $T(z)$ because it is closely related to the molecular number density $N(z)$, which is proportional to air pressure and the inverse of temperature, according to the well-known equation of state for air [*Penndorf*, 1957]. In addition, $\beta(\lambda, z)$ is influenced by the air moisture conditions, which can appreciably modify the refractive index of moist air [*Ciddor*, 1996, 2002] and the King factor [*Tomasi et al.*, 2005]. To define these dependence features, calculations of $\beta(\lambda, z)$ were performed at wavelengths equal to 0.30, 0.40, 0.50, 0.70, 1.00, and 4.00 $\mu$m for the vertical profiles of $p(z)$, $T(z)$, and RH$(z)$ determined using (1) the average 10 day data derived from the 12 year radiosounding measurement set taken at Terra Nova Bay in Antarctica, from October to February [*Tomasi et al.*, 2004], from the surface level up to 20 km height and (2) the subarctic summer (July, 60°N) model [*Anderson et al.*, 1986] profiles throughout the height range from 20 to 120 km. The vertical profiles of $\beta(\lambda, z)$ were found to decrease as a function of height at all wavelengths, assuming values equal to (1) about 6% of $\beta(\lambda, 0)$ at the 20 km height and (2) lower than 0.4% of $\beta(\lambda, 0)$ at 40 km. These findings show very clearly that the main part of Rayleigh-scattering effects on solar radiation observed at polar sites takes place in the troposphere and the lower stratosphere, i.e., below 40 km. Calculations of ROD at the 0.50 $\mu$m wavelength, performed within the various regions of the atmosphere, indicate that an atmospheric contribution equal to 46.6% of the total atmospheric ROD is given by the lower tropospheric layer, between sea level and 5 km, with relative contributions of 27.2% due to the 5−10 km layer, 20.7% due to the 10−20 km layer, 4.3% due to
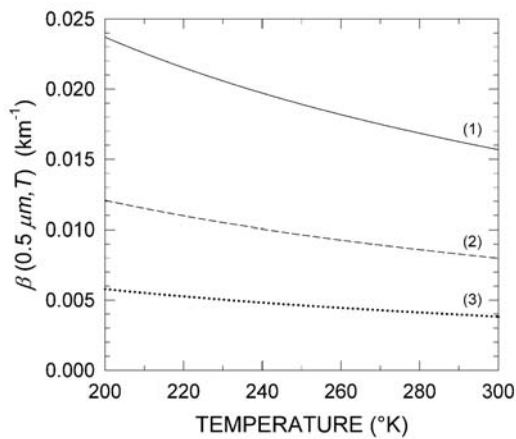
**Figure 2.** Values of Rayleigh-scattering coefficient $\beta(0.50 \ \mu m)$ as a function of air temperature $T$ throughout the $200-300$ K range, calculated at three tropospheric levels: curve 1 refers to the sea level, with $p = 980$ hPa and RH = 50%; curve 2 refers to 5 km altitude, with $p = 500$ hPa and RH = 30%; and curve 3 refers to 10 km altitude, with $p = 240$ hPa and RH = 20%.

the $20-30$ km layer, 0.9% due to the $30-40$ km layer, and 0.3% due only to the upper atmosphere. The above calculations show also that ratio $\beta(\lambda, z)/p(z)$ assumes rather stable values at the various heights, increasing from less than $1.7 \times 10^{-5} \ km^{-1} \ hPa^{-1}$ at sea level to more than $2.2 \times 10^{-5} \ km^{-1} \ hPa^{-1}$ at the tropopause level and decreasing gradually through the stratosphere until reaching a value lower than $1.8 \times 10^{-5} \ km^{-1} \ hPa^{-1}$ at the stratopause ($\sim$50 km). These findings confirm the close dependence of $\beta(\lambda, z)$ on air pressure $p(z)$ at all tropospheric and stratospheric levels of the polar atmosphere, with variations in the proportionality factor which are mainly related to air temperature.

[13] In order to investigate the dependence features of $\beta(\lambda, z)$ on temperature $T$ for different values of $p$ and RH, calculations of $\beta(\lambda, T, p, RH)$ were made at various wavelengths for values of $T$ ranging between 200 and 300 K and the following pairs of $p$ and RH values: (1) $p = 980$ hPa and RH = 50%, to simulate the sea-level air pressure and moisture conditions, (2) $p = 500$ hPa and RH = 30%, to represent the average meteorological conditions at the 5 km height, and (3) $p = 240$ hPa and RH = 20%, to represent the 10 km height conditions.

[14] The values of $\beta(\lambda)$ obtained at wavelength $\lambda = 0.50 \ \mu m$ for the three above-selected levels are given in Figure 2 over the $200-300$ K temperature range, showing that $\beta(0.50 \ \mu m)$ decreases by about 34% at all the tropospheric levels as $T$ increases from 200 to 300 K. The results indicate that this coefficient varies with ambient temperature similarly at all tropospheric levels. In order to quantify this behavior, the percentage slope coefficient $\gamma$ of parameter $\beta$, expressed as the ratio $(d\beta/dT)/\beta$, was calculated over the range $200 \leq T \leq 300$ K for the three curves shown in Figure 2. It was found that $\gamma$ varies from less than $-0.50\%$ $K^{-1}$ at $T = 200$ K to $-0.39\%$ $K^{-1}$ at $T = 260$ K. Coefficient $\gamma$ decreases gradually above 270 K, with differences of about 0.01% $K^{-1}$ between 280 and 300 K. Therefore, differences in $\gamma$ are rarely observed in the polar atmospheres, only on warm summer days with $T_o > 280$ K.

[15] To study the dependence of Rayleigh-scattering on air moisture, values of $\beta(0.50 \ \mu m, 270$ K) were calculated for pressure $p = 980$ hPa and relative humidity RH equal to 20%, 40%, and 60%. These values were found to increase by about 0.03% as RH decreases from 40% to 20% and decrease by 0.03% as RH increases from 40% to 60%, showing that changes in $\beta(\lambda)$ due to variations in RH are negligible for the normal range of humidity in polar regions. Calculations of $\beta(0.50 \ \mu m, 270$ K) were also made at $p = 980$ hPa and RH = 40% for two values of $CO_2$ volume concentration $C$, equal to 330 and 380 ppmv. This increase in $C$ (observed over the last 50 years) leads to an increase in $\beta(0.50 \ \mu m, 270$ K) of no more than 0.006%, which is a totally negligible effect.

[16] The above results confirm that coefficient $\beta(\lambda, z)$ can vary significantly with air pressure and temperature, while the seasonal and daily changes in air moisture and $CO_2$ concentrations result in negligible variations. Considering these findings, it is useful to determine the variations of Rayleigh-scattering parameters as a function of $p(z)$ and $T(z)$ at Arctic and Antarctic sites on the basis of vertical profiles measured at different high-latitude locations and over the annual cycle. Our objective is to characterize the polar atmospheric profiles of these parameters and evaluate the sensitivity of ROD to the latitudinal and altitudinal variations that occur from season to season. To accomplish this, we have selected the following sites between 70° and 90° of latitude and from sea level to over 3000 m: (1) YCB Cambridge Bay and Resolute (Nunavut, Canada), Danmarkshavn (Greenland), Eureka and Alert (Northwest Territories, Canada), and Ny-Ålesund (Svalbard Islands) in the Arctic, and (2) Neumayer, Mario Zucchelli, McMurdo, Dome C, and South Pole in Antarctica.

## 3. Selection and Analysis of Radiosounding Measurements Obtained in Polar Regions

[17] Six multiyear sets of radiosounding measurements made at Arctic sites and five multiyear sets obtained at Antarctic sites were selected for determining the seasonally varying profiles of pressure, temperature, and humidity at polar latitudes. Five of the six Arctic data sets were downloaded from the World Meteorological Organization (WMO) database of the University of Wyoming (http://weather.uwyo.edu/upperair/sounding.html). The sixth Arctic data set, for Ny-Ålesund, was provided by the Alfred Wegener Institut for Polar and Marine Research (AWI), Bremerhaven, Germany. These six Arctic data sets and the five selected to represent Antarctica are listed with pertinent descriptions in Table 1.

### 3.1. Selection of Clear-Sky Radiosounding Data

[18] Wavelength-dependent evaluations of the Rayleigh-scattering parameter ROD($\lambda$) are made in order to correct measurements of total atmospheric optical depth for attenuation due to molecular scattering during clear-sky periods. Thus, only soundings made during cloudless periods are examined here. Selections were made on the basis of RH profiles, whereby any profile having RH $\geq$ 80% at one or more significant levels was discarded, with exception of South Pole, where the threshold was set at RH = 85% for

**Table 1.** List of the Radiosounding Stations, Vaisala Radiosonde Models, Measurement Periods, Total Number of Examined Radiosoundings, Total Number of Clear-Sky Radiosoundings Selected for the Present Analysis, and Number of Monthly Radiosoundings Used in the Present Calculations of Rayleigh-Scattering Parameters

| Stations With Their Coordinates | Vaisala Radiosonde Models | Radiosounding Period | Radiosounding Total Number | Overall Number of Selected Clear-Sky Radiosoundings | Number of Monthly Radiosounding Sets |
|---|---|---|---|---|---|
| YCB Cambridge Bay (69°08′N, 105°04′W, 25 m above MSL), Nunavut, Canada | RS80A | January 2000 to December 2003 | 2838 | 240 | 12 |
| Resolute (74°43′N, 94°59′W, 40 m above MSL) Cornwallis Island, Nunavut, Canada) | RS90 | January 2000 to December 2003 | 2860 | 240 | 12 |
| Danmarkshavn (76°46′N, 18°46′E, 12 m above MSL), Greenland | RS80A RS90 | January 2000–December 2003 | 2615 | 240 | 12 |
| Eureka (79°59′N, 85°56′W, 10 m above MSL), Northwest Territories, Canada | RS90 | January 2000–December 2003 | 2884 | 240 | 12 |
| Alert (82°30′N, 62°21′W, 65 m above MSL), Northwest Territories, Canada | RS90 | January 2000–December 2003 | 2871 | 240 | 12 |
| Ny-Ålesund AWIPEV station (78°54′N; 11°53′E; 11 m above MSL), Svalbard, Norway | RS80A RS90 | April 2000–September 2003 | 750 | 120 | 6 (from April to September) |
| Neumayer (70°39′S, 8°15′W, 42 m above MSL), Antarctic coast | RS80A RS90 | January 2000–January 2003 | 685 | 120 | 6 (from October to March) |
| Mario Zucchelli (74°42′S, 164°07′E, 55 m above MSL), Antarctic coast | RS80A | January 2000–December 2003 | 675 | 100 | 5 (from October to February) |
| McMurdo (77°51′S, 166°40′E, 24 m above MSL), Antarctic coast | RS80A | January 2000–December 2003 | 1858 | 240 | 12 |
| Dome C (75°06′S, 123°21′E, 3233 m above MSL), Antarctic Plateau | RS92 | January 2005–December 2006 | 445 | 240 | 12 |
| South Pole (89°59′S, 24°48′W, 2835 m above MSL), Antarctic Plateau | RS80A RS80H RS90 | August 2001–December 2003 | 1278 | 240 | 12 |

**Table 2.** Extreme Values of Surface Temperature $T_o$ (K) Found for the Monthly Sets of Radiosoundings Selected at the Various Arctic and Antarctic Sites[a]

| Station | Month | | | | | | | | | | | |
|---|---|---|---|---|---|---|---|---|---|---|---|---|
| | Jan | Feb | Mar | Apr | May | Jun | Jul | Aug | Sep | Oct | Nov | Dec |
| YCB Cambridge Bay | 233.3–249.7 | 229.9–247.7 | 231.7–253.1 | 239.9–262.5 | 249.3–274.0 | 263.5–287.6 | 276.4–293.0 | 273.8–290.6 | 260.5–285.4 | 250.7–277.0 | 238.9–252.1 | 234.9–251.7 |
| Resolute | 235.9–250.7 | 226.1–240.5 | 233.9–256.9 | 238.9–259.5 | 255.1–294.1 | 256.1–294.1 | 276.2–294.5 | 269.5–281.4 | 261.7–274.8 | 248.3–266.1 | 240.7–257.1 | 233.7–255.1 |
| Danmarkshavn | 236.1–263.1 | 241.7–263.3 | 237.5–259.1 | 245.9–271.1 | 259.3–274.8 | 268.7–285.8 | 278.2–287.2 | 274.4–285.2 | 265.7–277.8 | 256.5–271.3 | 248.7–263.1 | 241.7–261.1 |
| Eureka | 230.1–250.5 | 223.1–252.9 | 227.3–246.9 | 235.1–259.3 | 245.1–269.5 | 268.3–284.6 | 276.8–289.2 | 270.1–287.4 | 253.9–275.6 | 244.1–266.5 | 234.1–254.7 | 230.3–253.3 |
| Alert | 233.9–258.5 | 232.1–247.3 | 230.9–259.5 | 235.1–257.1 | 252.7–270.3 | 269.3–286.2 | 276.4–287.4 | 272.7–283.4 | 255.3–274.8 | 250.9–269.9 | 239.7–253.7 | 235.5–258.5 |
| Ny-Ålesund | — | — | — | 251.4–273.0 | 263.0–276.2 | 272.2–280.6 | 276.7–283.4 | 275.0–285.3 | 265.4–277.6 | — | — | — |
| Neumayer | 262.7–275.1 | 253.0–267.4 | 247.3–265.1 | — | — | — | — | — | — | 240.5–261.6 | 251.8–265.1 | 262.1–273.9 |
| Mario Zucchelli | 269.7–280.6 | 263.0–271.3 | — | — | — | — | — | — | — | 250.9–267.0 | 261.4–282.0 | 267.4–279.9 |
| McMurdo | 262.3–279.4 | 261.7–271.3 | 245.5–263.5 | 243.1–259.1 | 244.7–258.3 | 238.5–252.5 | 235.9–255.3 | 231.7–252.1 | 238.9–255.9 | 248.7–267.5 | 252.7–271.3 | 262.3–279.8 |
| Dome C | 238.9–252.2 | 222.0–241.3 | 205.4–232.4 | 205.3–222.2 | 195.5–229.9 | 202.8–228.8 | 201.3–228.5 | 197.3–219.5 | 195.9–226.4 | 209.9–225.7 | 218.7–239.0 | 243.3–252.2 |
| South Pole | 240.3–251.4 | 224.8–241.9 | 217.2–238.5 | 207.9–241.8 | 210.2–238.8 | 204.5–224.0 | 205.6–230.5 | 200.4–228.2 | 206.9–232.1 | 215.3–233.4 | 229.8–241.3 | 231.4–250.7 |

[a]Temperature given in kelvins.
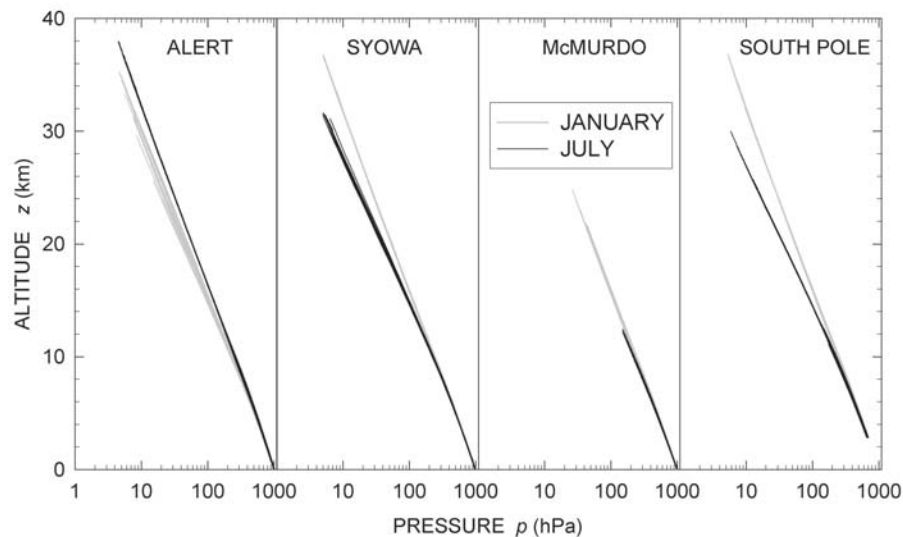
**Figure 3.** Comparison of the January (gray) and July (black) vertical profiles of air pressure $p(z)$ obtained for the monthly sets of selected radiosounding data recorded at Alert (82°30′N, 62°21′W, 65 m above mean sea level (MSL)), Syowa (69°00′S, 39°35′E, 29 m above MSL), McMurdo (77°51′S, 166°40′E, 24 m above MSL), and South Pole (89°59′S, 24°48′W, 2835 m above MSL).

March–June and September in order to collect the 20 radiosoundings needed for the analyses.

[19] Each set of 20 soundings per month was analyzed (1) to determine values of surface air temperature $T_o$, (2) to determine the range of $T_o$ for the various months, (3) to identify the profiles having extremes of $T_o$, and (4) to order profiles by monotonically increasing values of $T_o$. Following these steps, monthly sets consisting of 20 clear-sky radiosoundings were obtained for each of the 11 stations listed in Table 1, with extreme values of $T_o$ given in Table 2 for each month.

### 3.2. Correction of Radiosounding Data for Lag Errors and Dry Bias

[20] Each radiosounding downloaded from the Wyoming University database consists of values of $p(h)$, $T(h)$, and RH($h$) measured typically at some 150 significant levels of geopotential height $h$ in the troposphere and more than 400 levels in the stratosphere. The radiosoundings used at the Ny-Ålesund, Neumayer, and Mario Zucchelli stations provide measurements at some 300 significant levels in the troposphere and 500 levels in the stratosphere, while those carried out at the high-altitude stations of Dome C and South Pole provided data taken at more than 400 significant tropospheric levels and 1400 stratospheric levels.

[21] The vertical profiles of $p(z)$ were determined for each radiosounding using the original air pressure data and the values of geometrical height $z$, derived from those of $h$ through a correction factor depending on Earth's radius and sea-level acceleration gravity as a function of latitude. The temperature data given by the RS80A and RS80H radiosondes were corrected following (1) the procedure defined by *Tomasi et al.* [2006] on the basis of the *Luers and Eskridge* [1995] evaluations of various errors caused by heat lost and radiation exchanges between the Thermocap sensor and the surrounding environment. These data were subsequently corrected for the lag errors associated with the radiosonde balloon ascent rate, using the algorithm pro-

posed by *Tomasi et al.* [2004]. In the analysis of the temperature data given by the RS90 and RS92 radiosondes, the lag errors were neglected, according to *Luers* [1997].

[22] The measurements of RH were taken by Vaisala radiosondes equipped with various Humicap sensor models at numerous (at least 130) tropospheric levels and sometimes at some significant stratospheric levels. As pointed out by *Wang et al.* [2002], the RH data provided by the Humicap sensors are usually affected by significant dry biases, due to temperature dependence, chemical contamination, basic calibration models, sensor aging, ground check, and sensor arm heating. These errors were all corrected adopting the *Wang et al.* [2002] criteria. The procedure was completed with further corrections of the dry bias due to solar heating [*Turner et al.*, 2003; *Miloshevich et al.*, 2006] and the lag errors studied by *Miloshevich et al.* [2004], who proposed an appropriate correction procedure based on (1) a preliminary smoothing procedure, (2) a subsequent use of coefficients suitable for defining the most reliable time constants of the various humidity sensors, (3) the evaluation of corresponding lag correction terms, and (4) a final smoothing procedure of the RH vertical profile.

### 4. Seasonal Variations in the Vertical Profiles of Pressure and Temperature

[23] The vertical profiles of pressure $p(z)$, temperature $T(z)$, and relative humidity RH($z$) were determined for each radiosounding from the ground level to the highest significant levels reached by the Barocap, Thermocap, and Humicap sensors of the Vaisala radiosondes, respectively. In general, pressure and temperature data have been obtained up to altitudes of 30 km, while reliable data of RH > 2% have been obtained up to about 10 km altitudes only.

[24] Eight monthly sets of vertical profiles of $p(z)$ determined in January and July at Alert (in the Arctic) and Syowa, McMurdo, and South Pole (in Antarctica) are shown in Figure 3, within the altitude range from the
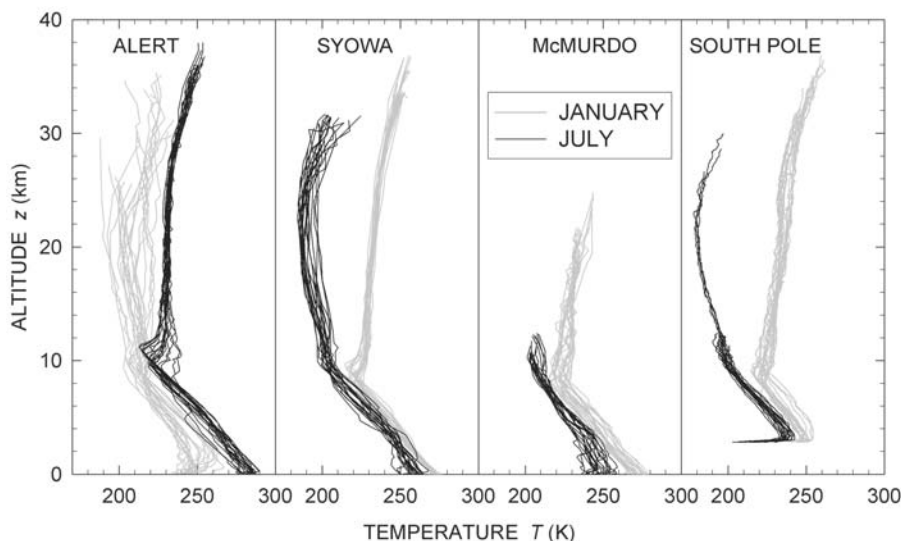
**Figure 4.** Comparison of the January (gray) and July (black) vertical profiles of air temperature $T(z)$ obtained for the monthly sets of selected radiosounding data recorded at Alert (82°30′N, 62°21′W, 65 m above MSL), Syowa (69°00′S, 39°35′E, 29 m above MSL), McMurdo (77°51′S, 166°40′E, 24 m above MSL), and South Pole (89°59′S, 24°48′W, 2835 m above MSL).

surface to stratospheric levels ranging between 20 and 40 km. It was decided to examine the radiosounding data measured at Syowa to compare the characteristics of the Antarctic atmosphere in January and July at 70°S latitude, since the radiosounding at Neumayer was performed only during the austral summer months. The two monthly data sets of pressure and temperature vertical profiles at Syowa were selected from a set of radiosounding measurements performed with the MEISEI RS2-91 radiosondes during the 4 year period from 2000 to 2003 and downloaded from the WMO database at the University of Wyoming. The comparison between the January and July profiles gives evidence of the opposite baric conditions of the upper troposphere and stratosphere during the local winter and summer periods. The vertical profiles observed at Alert in the winter months exhibit pressure values which start to appreciably diverge from those of July at altitudes ≥6 km and appear to be more variable in January than in July. On average, the January values were found to be lower than those observed in July, by 23% at 20 km and 28% at 30 km. At Syowa, the January values of air pressure determined up to altitudes of more than 30 km were found to be higher than those recorded in July by about 30% at 20 km and about twice those of July at 30 km. Comparable differences between the austral summer and winter conditions were found at McMurdo at the same tropospheric altitudes. The comparison between January and July data at McMurdo is incomplete because the vertical profiles of $p(z)$ measured at this site in July are missing for altitudes >12 km due to adverse meteorological conditions aloft during the austral winter. At South Pole, the January values are appreciably higher than for July at all stratospheric levels, by about 50% at 20 km and by more than twice at 30 km. The atmosphere above 10 km contributes >26% to values of ROD. Therefore, the variations in the vertical profiles of $p(z)$, shown in Figure 3, indicate that marked decreases in Rayleigh scat-

tering occur at all stratospheric levels when passing from summer to winter.

[25] The vertical profiles of $T(z)$ obtained at Alert, Syowa, McMurdo, and South Pole for the same four monthly sets presented in Figure 3 are shown in Figure 4 to represent the temperature characteristics of the Arctic atmosphere at ~80°N and those of the Antarctic atmosphere at ~70°S, ~80°S, and 90°S latitudes. The comparison shows that large seasonal variations in temperature take place within the troposphere and stratosphere when passing from winter to summer. Figure 4 also shows that the vertical profiles of $T(z)$ are subject to large day-to-day variations at all tropospheric and stratospheric levels. The average values of $T(z)$ measured at the four sites in January and July at the ground level and at some selected tropospheric and stratospheric altitudes are given in Table 3, together with the corresponding values of the differences $\Delta_{JJ}T(z)$, to give a measure of the average thermal excursions observed at various levels in January and July. There is a strong increase in the heating of the troposphere in both the Arctic and Antarctic atmospheres when passing from local winter to summer. Table 3 also lists estimates of the monthly difference $\delta_T$ between maximum and minimum temperatures observed at some tropospheric and stratospheric levels in January and July. Values of $\delta_T$ vary between 8 K and 27 K in the troposphere and between 2 K and more than 43 K in the lower stratosphere. Given that the volume Rayleigh-scattering coefficient decreases by 34% (Figure 2) as the temperature increases from 200 to 300 K, such marked changes in $T(z)$ occurring in the atmosphere are expected to cause variations of several percent in ROD, from one month to another, and even from day to day in some instances.

### 4.1. Evaluations of Pressure Effects

[26] The vertical profiles of $\beta(0.50 \ \mu m, z)$ were calculated with the *Tomasi et al.* [2005] algorithm for the vertical

**Table 3.** Monthly Average Values of Air Temperature $T(z)$ at Different Tropospheric and Stratospheric Levels, Measured in January and July at Alert, McMurdo, and South Pole, Together With the Corresponding January-to-July Thermal Variations $\Delta_{JJ}T(z)$ and the Monthly Estimates of Difference $\delta_T$ Between Maximum and Minimum Temperature Values Recorded in January and July at Various Altitudes Above Alert, McMurdo, and South Pole

| | Monthly Average Values of $T(z)$ (K) | | | | | | | | | | | |
|---|---|---|---|---|---|---|---|---|---|---|---|---|
| | Alert | | | Syowa | | | McMurdo | | | South Pole | | |
| Levels | Jan | Jul | $\Delta_{JJ}T(z)$ (K) | Jan | Jul | $\Delta_{JJ}T(z)$ (K) | Jan | Jul | $\Delta_{JJ}T(z)$ (K) | Jan | Jul | $\Delta_{JJ}T(z)$ (K) |
| Surface level | 242.7 | 282.9 | +40.2 | 272.8 | 258.1 | −14.7 | 273.1 | 245.3 | −27.8 | 247.3 | 213.4 | −33.9 |
| $z$ = 5 km | 234.6 | 254.9 | +20.3 | 241.5 | 233.1 | −8.4 | 241.8 | 228.3 | −13.5 | 241.5 | 229.8 | −11.7 |
| $z$ = 10 km | 212.2 | 222.7 | +10.5 | 225.3 | 203.4 | −21.9 | 222.9 | 206.4 | −16.5 | 223.5 | 199.1 | −24.4 |
| $z$ = 20 km | 206.2 | 230.6 | +24.4 | 232.3 | 190.0 | −42.3 | 235.0 | – | – | 234.8 | 180.9 | −53.9 |
| $z$ = 30 km | 218.0 | 237.8 | +19.8 | 242.4 | 204.5 | −37.9 | – | – | – | 243.2 | – | – |

| | Excursion Range $\delta_T$ (K) | | | | | | | |
|---|---|---|---|---|---|---|---|---|
| Levels | Jan | Jul | Jan | Jul | Jan | Jul | Jan | Jul |
| Surface level | 24.6 | 11.0 | 8.5 | 15.4 | 17.1 | 19.4 | 8.1 | 27.3 |
| $z$ = 5 km | 17.2 | 18.9 | 8.7 | 16.0 | 13.9 | 11.2 | 16.9 | 13.0 |
| $z$ = 10 km | 16.2 | 16.7 | 10.5 | 11.6 | 14.0 | 11.0 | 11.0 | 7.2 |
| $z$ = 20 km | 30.1 | 3.7 | 4.7 | 12.0 | 11.7 | – | 8.3 | 2.3 |
| $z$ = 30 km | 43.4 | 4.5 | 6.9 | 28.7 | – | – | 7.5 | – |

profiles of $p(z)$ and $T(z)$ measured at Alert and South Pole (see Figures 3 and 4), assuming RH = 1% at all stratospheric levels. Results shown in Figure 5 reveal large differences between the January and July vertical profiles of $\beta(0.50\ \mu m, z)$, in large part due to the variations in pressure that occur at stratospheric levels. Parameter $\beta(0.50\ \mu m, z)$ decreases with altitude by more than 2 orders of magnitude from the surface to 30 km in accordance with the vertical gradient of pressure. The January profiles at Alert are more variable than during July in correlation with features of air pressure shown in Figure 3. Similarly, the January South Pole profiles have higher values than during July, giving further evidence that air pressure is the most important variable influencing Rayleigh scattering.

[27] The analysis of air pressure data obtained using the Barocap sensor at the ground level and at altitudes of 5, 10, and 20 km on selected days at the 11 polar stations indicated that the ground-level pressure $p_o$ varies throughout the year between (1) about 985 and more than 1040 hPa at the Arctic stations, (2) about 950 and 1025 hPa at the coastal Antarctic sites, and (3) 620 and more than 700 hPa at the two Antarctic Plateau stations, with the annual extremes and average values of pressure given in Table 4. The time patterns of $p_o$ at the Arctic sites are rather stable throughout the year, while those measured at the upper levels exhibit a marked maximum in summer. The values of $p_o$ at the coastal Antarctic stations are also stable during the year, whereas the pressure values at 5 km describe a broad minimum during the austral winter. Values of $p(z)$ at 10 and 20 km exhibit less variability from January to March and are highly variable from October to December. Data for April–September at all stratospheric levels are lacking because of the failure of balloons entering extreme conditions within the Antarctic vortex during that period. Surface pressure $p_o$ at the two high-altitude Antarctic sites varies within ±20 hPa throughout the year, while pressure values at 5, 10, and 20 km levels tend to reach broad minima, particularly during the austral winter. These results suggest that variations in $p_o$ may be useful in quantifying the sensitivity of ROD to changes in the vertical structure of

the atmosphere that occur spatially and temporally at polar sites. However, the lack of stratospheric data for the Antarctic sites during winter prohibits a thorough evaluation of influences above 20 km. To overcome this limitation, we use the available standard vertical profiles of CIRA (COSPAR International Reference Atmosphere 1986, 0–120 km), which include profiles of pressure and temperature for 70°N, 80°N, 70°S, and 80°S latitudes over the 20–120 km altitude range (see the Web site http://badc.nerc.ac.uk/data/cira/).

### 4.2. Evaluations of Temperature Effects

[28] In order to assess the temperature effects on the Rayleigh-scattering coefficient, the vertical profiles of ratio $b(0.50\ \mu m, z)$ between coefficient $\beta(0.50\ \mu m, z)$ and $p(z)$ are presented in Figure 6 for the January and July soundings from Alert and South Pole, assuming RH = 1% at all levels
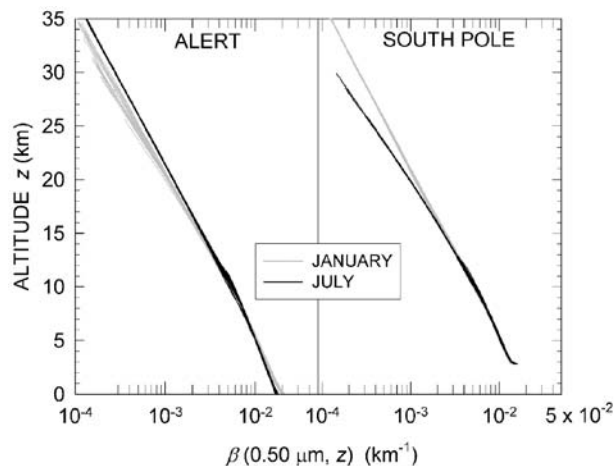


**Figure 5.** Vertical profiles of volume Rayleigh-scattering coefficient $\beta(0.50\ \mu m, z)$ calculated using the algorithm of *Tomasi et al.* [2005] for the January (gray) and July (black) monthly sets of 20 selected radiosoundings at (left) Alert and (right) South Pole.

**Table 4.** Multiyear Range and Average Values With Their Standard Deviations of Surface Pressure $p_o$ and Temperature $T_o$ Obtained for the Eight Latitudinal/Altitudinal Site Classes Characterizing the Ambient Conditions at the Selected Polar Sites

| Stations of the Eight Locales | Approximate Latitude | Multiyear Range of Ground-Level Pressure $p_o$ (hPa) | Multiyear Average Value $p_a$ of Ground-Level Pressure $p_o$ With Standard Deviation (hPa) | Multiyear Range of Ground-Level Temperature $T_o$ (K) | Multiyear Average Value $T_a$ of Ground-Level Temperature $T_o$ With Standard Deviation (K) |
|---|---|---|---|---|---|
| YCB Cambridge Bay | ~70°N | 988.0–1045.0 | 1013.4 ± 8.6 | 229.9–293.0 | 258.8 ± 17.8 |
| Resolute and Danmarkshavn | ~75°N | 982.0–1037.0 | 1010.1 ± 8.5 | 226.1–294.5 | 260.6 ± 14.8 |
| Eureka, Alert and Ny-Ålesund | ~80°N | 981.0–1043.0 | 1011.3 ± 9.9 | 223.1–289.2 | 260.1 ± 16.6 |
| Neumayer[a] | ~70°S | 966.1–1003.0 | 985.3 ± 8.0 | 240.5–275.1 | 260.2 ± 7.1 |
| Mario Zucchelli[b] | ~75°S | 950.5–1002.0 | 981.9 ± 9.9 | 250.9–282.0 | 268.6 ± 6.6 |
| McMurdo | ~80°S | 964.0–1025.0 | 988.8 ± 10.8 | 231.7–279.8 | 256.3 ± 11.5 |
| Dome C | ~75°S | 619.4–665.4 | 644.4 ± 9.6 | 195.5–252.2 | 221.3 ± 15.1 |
| South Pole | ~90°S | 656.8–707.6 | 683.5 ± 8.5 | 200.4–251.4 | 227.2 ± 12.7 |

[a]Over the 6 month period from October to March (austral summer) only.
[b]Over the 5 month period from October to February (austral summer) only.

above 10 km. Through such a normalization, the pressure effects on Rayleigh scattering are effectively removed, revealing effect solely because of changes in temperature. Figure 6 shows that decreases in temperature at Alert from July to January lead to increases in $\beta(0.50~\mu m, z)$ by more than 10% at the surface and within the troposphere, with greater variations in the stratosphere. At South Pole, the January to July temperature variations are estimated to produce relative changes of $\leq 10\%$ within the troposphere, but increasing effects at higher altitudes and exceeding 30% above 15 km.

[29] The analysis of air temperature data measured by the Thermocap sensor at the surface and at the 5, 10, and 20 km levels on selected days at the Arctic and Antarctic sites indicated that the ground-level values of $T_o$ varied between (1) 225 K and more than 290 K in the Arctic, (2) 232 and 282 K at the coastal sites in Antarctica, and (3) 195 and 252 K on the Antarctic Plateau, with statistical information given in Table 4. The annual range in $T_o$ observed at the Arctic sites was nearly 70 K, and the annual average temperature

(at the six locations examined) was about 260 K. The range in $T_o$ at the Antarctic coastal stations was about 50 K, with annual mean close to 260 K. Annual variations of about 56 K and 52 K characterize Dome C and South Pole (90°S), respectively. More precisely, the values of $T_o$ at the Arctic sites were found to exhibit a marked maximum during the boreal summer, peaking at around 280 K. A maximum also occurs at 5 km and another less pronounced one is evident at 10 km. At 20 km, a distinct maximum is observed from May to October. Given the similarities at all levels, it appears that $T_o$ may be useful for parameterizing temperature effects on ROD through the vertical column of the Arctic atmosphere.

[30] The Antarctic coastal data reveal temperature minima in July and August, and similar features at 5 and 10 km. At the 20 km altitude, temperatures from October through December vary between 190 and 250 K. Such a wide range suggests that different heat exchange processes take place within the vortex from year to year. Considering the scarcity of observational data obtained from soundings at high altitudes, from April to September, it was decided to use the CIRA standard profiles for estimating ROD during the austral winter months. At Dome C and South Pole, values of $T_o$ are very low during the austral winter, while similar but less pronounced features characterize the upper levels, which have marked minima at both 10 and 20 km.

### 4.3. Evaluations of Relative Humidity Effects

[31] The vertical profiles of RH selected in section 3.2 for the various monthly sets were found to vary largely with altitude at the 11 selected polar sites. The moisture input inserted into the algorithm of *Tomasi et al.* [2005] used to calculate the scattering parameters is expressed in terms of water vapor partial pressure, which varies as a function of temperature and RH. To evaluate the effects of variable RH within the troposphere, in the 10–70%, range, a comparison is shown in Figure 7 between the vertical profiles of parameter $B_1(\lambda, z)$ at wavelength $\lambda = 0.50~\mu m$, determined at McMurdo for January and July. Parameter $B_1(0.50~\mu m, z)$ is given by the ratio



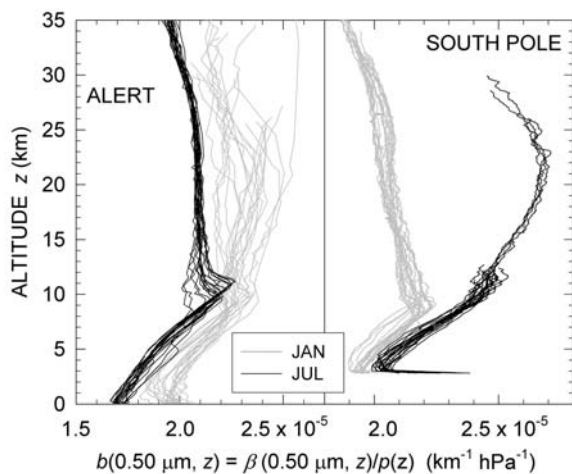**Figure 6.** Vertical profiles of the ratio $\beta(0.50~\mu m, z)/p(z)$ calculated for the January (gray) and July (black) monthly sets of 20 selected radiosoundings at (left) Alert and (right) South Pole, assuming RH = 1% at all levels higher than 10 km.

$$B_1(0.50~\mu m, z) = \beta[\lambda, p(z), T(z), RH = 10\%]$$
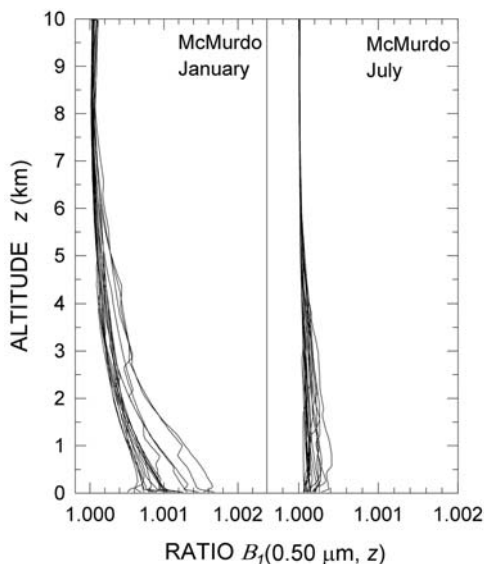$$/\beta[0.50~\mu m, p(z), T(z), RH = 70\%], \qquad (2)$$

**Figure 7.** Comparison of the 20 vertical profiles of ratio $B_1(0.50 \mu m, z)$ in equation (2) calculated for the vertical profiles of $p(z)$ and $T(z)$ obtained at all levels from surface to 10 km for the sets of 20 selected radiosoundings performed at McMurdo in (left) January and (right) July.

where the volume Rayleigh-scattering coefficient $\beta(0.50 \mu m, z)$ is calculated for the vertical profiles of pressure and temperature measured at McMurdo, as shown in Figures 3 and 4, respectively, in which RH = 10% at all levels in the numerator and RH = 70% at all levels in the denominator. The ratio $B_1(0.50 \mu m, z)$ is more variable in the lower troposphere than above 5 km. At the ground level, variations are within ±0.05% for summer conditions (January) and within ±0.01% during winter (July). The comparison in Figure 7 shows clearly that even large variations in RH result in negligible changes in volume Rayleigh-scattering coefficient at tropospheric levels.

## 5. Determination of Vertical Profiles of Pressure, Temperature, and RH in Polar Atmospheres

[32] The values presented in Figures 5 and 6 show that the seasonal variations in $p(z)$ and $T(z)$ cause significant changes in $\beta(0.50 \mu m, z)$, which are proportional to pressure and inversely proportional to air temperature at all levels. In order to compute accurate values of ROD($\lambda$) using the algorithm of *Tomasi et al.* [2005], vertical profiles of $p(z)$, $T(z)$, and RH($z$) from the surface to 50 km altitude are needed. To satisfy this requirement, we merged the measured soundings up to 20 km with the upper-level profiles taken from the CIRA standard atmospheres given for 70°N, 80°N, 70°S, and 80°S latitudes, thus providing complete profiles for all locations and months for subsequent analyses. The main characteristics of the CIRA monthly mean vertical profiles of $p(z)$ and $T(z)$ are shown in Figures 8a and 9a, respectively. Supplemental monthly mean vertical profiles of $p(z)$ and $T(z)$ relative to the 75°N, 75°S, and 90°S latitudes were determined through some simple averaging and extrapolation procedures applied to the original CIRA profiles. They are shown in Figures 8b

and 9b, wherein (1) those at 75°N latitude were calculated by averaging for each month the pair of CIRA monthly mean vertical profiles at the 70°N and 80°N latitudes and then used to complete the monthly mean vertical profiles derived from the radiosoundings of Resolute and Danmarkshavn; (2) those at 75°S were calculated by averaging for each month the pair of CIRA monthly mean vertical profiles shown in Figure 9a for the 70°S and 80°S latitudes, and then used to complete the monthly mean vertical profiles obtained from the radiosoundings made at the Mario Zucchelli and Dome C stations; and (3) the monthly mean vertical profiles at 90°S latitude were obtained for each month through extrapolation to the South Pole latitude of the data given by the CIRA monthly vertical profiles at the 70°S and 80°S latitudes and used for integrating the vertical profiles measured with the radiosondes at South Pole. The vertical profiles of $p(z)$ shown in Figures 8a and 8b present marked month-to-month variations in the altitude range from 20 to 85 km above some Arctic and Antarctic sites. Considering that the atmospheric column above 40 km contributes, on average, only about 0.3% to ROD, the effects of seasonal variations in $p(z)$ at high altitudes are negligible.

[33] All the vertical profiles of $T(z)$ shown in Figures 9a and 9b exhibit considerable month-to-month variations, which are especially large between 20 and 60 km and from 70 to 100 km. As was evidenced in Figure 6, temperature
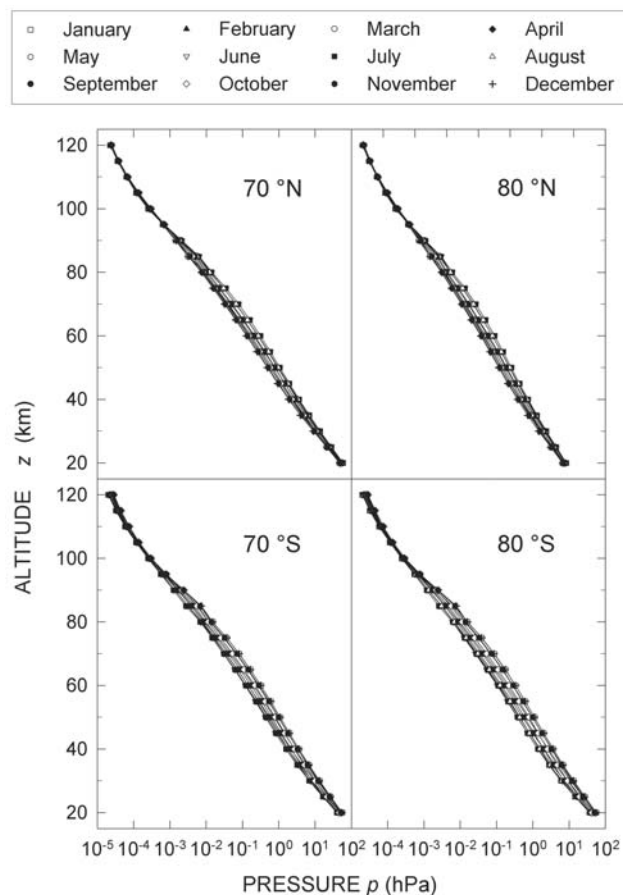


**Figure 8a.** Monthly mean vertical profiles of pressure $p(z)$ given by the CIRA atmospheric models in the altitude range from 20 to 120 km, at 70°N, 80°N, 70°S, and 80°S latitudes.
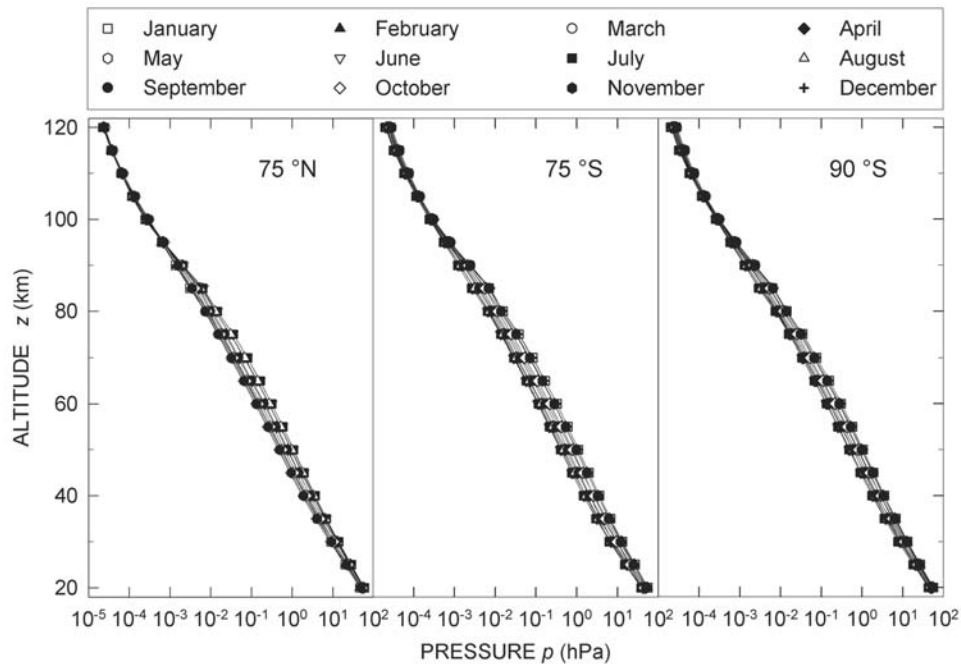
**Figure 8b.** (left) Monthly mean vertical profiles of pressure $p(z)$ obtained at the 75°N latitude in the 20–120 km altitude range by averaging each monthly pair of mean vertical profiles given by the CIRA atmospheric models at 70°N and 80°N latitudes. (middle) As in the left plot, for the monthly mean vertical profiles of pressure $p(z)$ at 75°S latitude obtained by averaging the monthly mean vertical profiles of the 70°S and 80°S CIRA atmospheric models. Right: as in the left part, for the monthly mean vertical profiles of pressure $p(z)$ at 90°S obtained through extrapolation in latitude of the 70°S and 80°S CIRA monthly mean vertical profiles.

effects on ROD at stratospheric levels, 15–30 km, cannot be neglected. In general, the atmospheric layer from 20 to 40 km contributes about 5% to the total value of ROD at polar latitudes. The effects of temperature variations at even higher altitudes are insignificant.

[34] The virtue in merging observational data with the CIRA model profiles of temperature is illustrated in Figure 10 for a selection of months. We found good agreement for the overlapping levels, which suggests that the CIRA profiles of $T(z)$ can be used to evaluate ROD at all stratospheric and mesospheric levels, where data are lacking.

[35] As explained in section 2.2, moisture effects on the Rayleigh-scattering coefficient are negligible at all wavelengths. However, in order to complete the radiosounding database, to include the monthly mean vertical profiles of water vapor mixing ratio $Q(z)$, remote sensing and satellite observations in the polar regions, above 8 km, were assimilated, noting that RH data measured by the Humicap sensors mounted on the radiosondes are reliable only below 8–10 km [*Wang et al.*, 2002; *Turner et al.*, 2003; *Miloshevich et al.*, 2004, 2006; *Tomasi et al.*, 2004, 2006]. Monthly mean vertical profiles of $Q(z)$ were calculated for altitudes above 8 km for the 70°N–80°N and 70°S–80°S zones and for 90°S (South Pole) by examining the water vapor mixing ratio measurements performed with different techniques in the Arctic and Antarctica and at South Pole.

[36] The moisture data in the Arctic region were derived from stratospheric measurements made during (1) the Limb Infrared Monitor of the Stratosphere Experiment (LIMSE)

retrieved using the Nimbus 7 satellite [*Russell et al.*, 1984], (2) the Halogen Occultation Experiment (HALOE) made with a solar occultation limb infrared sounder onboard the UARS satellite [*Harries et al.*, 1996], and the HALOE observations recorded from 1991 to 2000 [*Randel et al.*, 2001], (3) the experiment made with the Microwave Limb Sounder onboard the Upper Atmosphere Research Satellite (UARS) platform [*Lahoz et al.*, 1996], (4) the Stratospheric Aerosol and Gas Experiment (SAGE II) onboard the Earth Radiation Budget Satellite (ERBS) [*Chiou et al.*, 1997] over more than 5 years, (5) the experiment made with the Airborne Millimeter- and Submillimeter-Wave Observing System (AMSWOS) onboard the Learjet of the Swiss Air Force [*Peter*, 1998], (6) an Arctic campaign at Ny Ålesund, performed using balloon-borne frost point hygrometers [*Müller et al.*, 2003a, 2003b], and (7) a campaign carried out in 1992 and 1993, in which data from the Microwave Limb Sounder [*Morrey and Harwood*, 1998] were analyzed.

[37] In Antarctica, the water vapor mixing ratio measurements were derived from (1) LIMSE [*Russell et al.*, 1984], (2) HALOE [*Harries et al.*, 1996; *Randel et al.*, 2001], (3) the UARS experiment using the Microwave Limb Sounder [*Lahoz et al.*, 1996], (4) the SAGE II experiment [*Chiou et al.*, 1997; *Rind et al.*, 1993], (5) the AMSWOS experiment [*Peter*, 1998], and (6) the Microwave Limb Sounder campaign in winter months of 1992 [*Morrey and Harwood*, 1998]. The South Pole measurements of water vapor mixing ratio were obtained from (1) frost point sounding observations [*Rosen et al.*, 1991] and (2) ground-
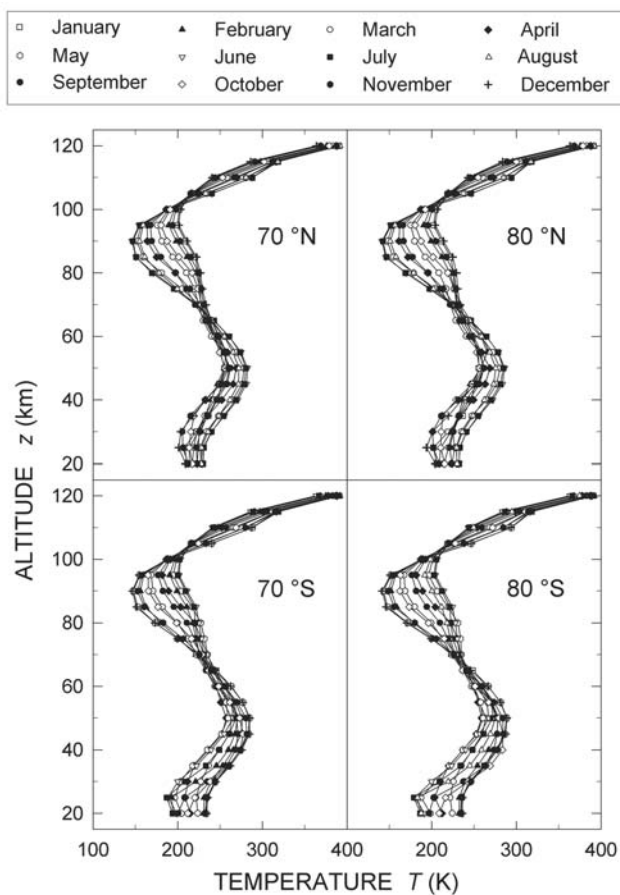
**Figure 9a.** Monthly mean vertical profiles of temperature $T(z)$ given by the CIRA atmospheric models in the altitude range from 20 to 120 km, at 70°N, 80°N, 70°S, and 80°S latitudes.

based lidar measurements [*Fiocco et al.*, 1996; *Cacciani et al.*, 1997]. As shown in Figure 11, the vertical profiles of $Q(z)$ obtained from the above satellite and remote-sensing experiments cover mainly the altitude range from 8 to 40 km and, in some cases, reach altitudes above 60 km. These profiles were completed by combining them with the vertical profile of $Q(z)$ defined in the subarctic winter and summer standard atmosphere models [*Anderson et al.*, 1986] shown in Figure 11 for altitudes above 30 km. Finally, in order to account for $CO_2$ effects on ROD, our models assume molecular concentration $C(z)$ of $CO_2$ equal to 380 ppmv from the surface to 75 km, according to the surface-level measurements of $CO_2$ concentration (Appendix A) obtained at various Arctic and Antarctic stations and the vertical distribution features adopted by *Anderson et al.* [1986], with monotonically decreasing values above, to reach a value equal to 40 ppmv at 120 km.

## 6. An Algorithm to Compute the Rayleigh-Scattering Optical Depth as a Function of Surface Temperature at Polar Latitudes

[38] Calculations of ROD($\lambda$) were performed at 88 wavelengths from 0.20 to 4 $\mu$m using the algorithm of *Tomasi et*

*al.* [2005] for the sets of vertical profiles of $p(z)$, $T(z)$, and RH($z$) obtained above, assuming (1) the monthly mean vertical profiles of $p(z)$ and $T(z)$ given by the CIRA models, (2) the monthly mean vertical profiles of RH($z$) derived from the monthly vertical profiles of water vapor mixing ratio $Q(z)$ shown in Figure 11, and (3) the vertical profiles of RH($z$) defined in the subarctic summer and subarctic winter models [*Anderson et al.*, 1986] in the upper part of the atmosphere. The calculations were made for eight radio-sounding data sets, of which (1) four correspond to YCB Cambridge Bay (~70°N), McMurdo (~80°S), Dome C (~75°S), and South Pole (90°S) stations, each consisting of 240 radiosoundings, (2) one consists of 480 radiosoundings obtained at Resolute and Danmarkshavn stations (both at latitudes close to 75°N), (3) one consists of 600 radiosoundings assimilated from Eureka, Alert, and Ny-Ålesund stations (all at latitudes close to 80°N), (4) one consists of 120 radiosoundings obtained at Neumayer (~70°S), and (5) one consists of 100 radiosoundings carried out at the Mario Zucchelli (~75°S) station.

[39] Table 4 lists the 4 year averages of surface pressure $p_a$ and temperature $T_a$ at the various locales selected above. Using the value of surface pressure $p_o$ relative to each radiosounding, all the values of ROD obtained for the integrated vertical profiles of $p(z)$, $T(z)$, and RH($z$) were multiplied by ratio $(p_a/p_o)$ to obtain values of ROD normalized to the aforementioned average values of $p_a$. These mean values of ROD($\lambda$) calculated for each wavelength, 0.20 to 4.0 $\mu$m, and each of the locales are listed in Table 5.

[40] To corroborate our results, the values of ROD(0.50 $\mu$m, $p_a$, $T_a$) given in Table 5 were normalized to the surface-level standard pressure $p_s = 1013.25$ hPa, by multiplying them by $p_s/p_a$, and were then compared with values of ROD(0.50 $\mu$m, $p_s$, $T_s$) reported by other investigators [*Bucholtz*, 1995; *Bodhaine et al.*, 1999; *Tomasi et al.*, 2005] for some atmospheric models defined at 45°N and 60°N [*Anderson et al.*, 1986]. The corresponding ratios between the present mean values of ROD(0.50 $\mu$m) in Table 5 and those given by the abovementioned authors (all normalized to $p_s = 1013.25$ hPa) are given in Table 6. They indicate that the present evaluations of ROD at the 0.50 $\mu$m wavelength differ from (1) those calculated by *Bucholtz* [1995] for the subarctic summer 60°N and subarctic winter 60°N models by percentages between −0.16% and +0.48%; (2) those calculated by *Bodhaine et al.* [1999] for the 45°N sea-level atmosphere above Mauna Loa (Hawaii) by percentages between −0.13% and +0.23%; and (3) those calculated by *Tomasi et al.* [2005] between −0.08% and +0.64%. These differences turn out to be comparable with the relative variations of ROD due to the differences in the vertical profiles of pressure estimated by *Bréon* [1998] to give variations in ROD of no more than 0.5% on passing from one standard atmosphere model to another. The substantial agreement in Table 6 between the results obtained for polar atmospheres and those for standard atmospheres arises from the fact that the polar calculations of ROD were made for annual average pressure and temperature conditions of the polar atmosphere, which differ significantly from those of the standard atmospheres within the lower part of the troposphere. The values of ROD(0.50 $\mu$m) normalized by $p_a$ are shown in Figure 12 as a function of $T_o$ separately for
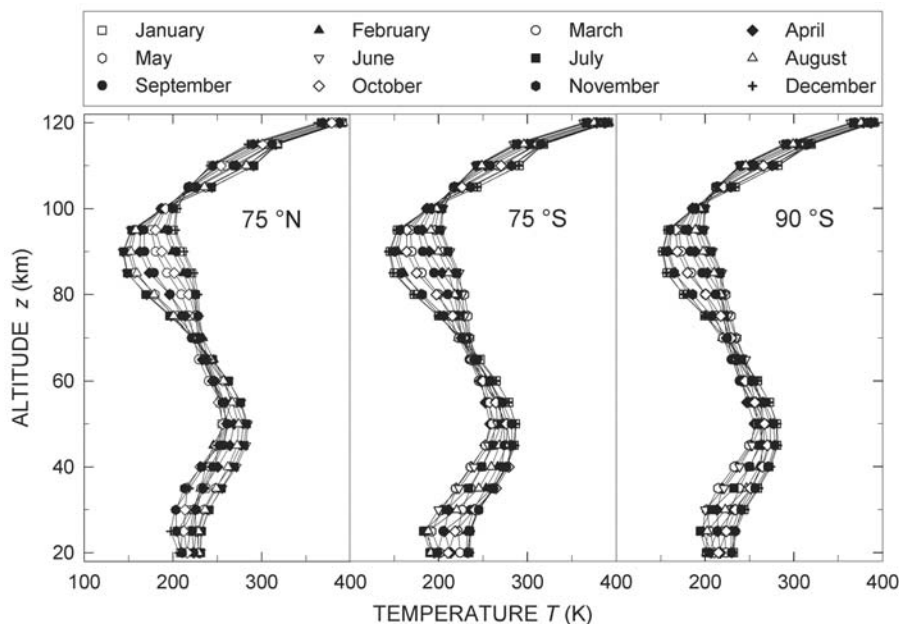
**Figure 9b.** (left) Monthly mean vertical profiles of temperature $T(z)$ obtained at the 75°N latitude in the 20–120 km altitude range by averaging each monthly pair of mean vertical profiles given by the CIRA atmospheric models at 70°N and 80°N latitudes. (middle) As in the left plot but for the monthly mean vertical profiles of air temperature $T(z)$ at 75°S latitude obtained by averaging the pairs of monthly mean vertical profiles of the 70°S and 80°S CIRA atmospheric models. (right) As in the left plot but for the monthly mean vertical profiles of temperature $T(z)$ at 90°S obtained through extrapolation in latitude of the 70°S and 80°S CIRA monthly mean vertical profiles.

each of the eight locales defined in Table 5. Results reveal very small discrepancies for given values of $T_o$. The scatter, defined as three standard deviations divided by the yearly average, is within ±0.4% at 70°N and 80°N, ±0.5% at 75°N, ±0.3% at 70°S, ±0.5% at 75°S, ±0.8% at 80°S, and ±1.0% at Dome C (75°S) and ±1.4% at South Pole (90°S).

[41] The regression lines exhibit the positive slope coefficient $\chi(\lambda)$ at all the Arctic stations and at the Mario Zucchelli and McMurdo stations in Antarctica. Conversely, negative values of $\chi(\lambda)$ were found at Neumayer (∼70°S) and the two Antarctic Plateau sites. Table 7 presents the values of the relative slope coefficient $k(\lambda)$ determined per unit value of ROD($\lambda$) at wavelengths of 0.20, 0.25, 0.30, 0.50, 1.00, 2.00, 3.00, and 4.00 $\mu$m, where $k(\lambda)$ is obtained by dividing $\chi(\lambda)$ by the corresponding values of ROD($\lambda, p_a, T_a$). The values of $k(\lambda)$ are similar at each location and decrease by <1% over the spectral range.

[42] As noted in Table 4, the annual range of $T_o$ considered for the calculations of ROD(0.50 $\mu$m) at the Arctic sites varied between 63 and 68 K and, hence, was larger than those observed in Antarctica: ∼48 K at McMurdo, ∼57 K at Dome C, and ∼51 K at South Pole. Conversely, the annual range of temperature at 20 km was 21–28 K only at the Arctic sites, from winter to summer, and ∼50 K at McMurdo, ∼45 K at Dome C, and ∼31 K at South Pole. The existence of intense surface-based temperature inversions at the South Pole and Dome C sites does not satisfactorily explain the observed decrease in ROD($\lambda$) as $T_o$ increases from its winter minimum to summer maximum.

A plausible explanation for the negative values of $\chi(\lambda)$ in Figure 12 and of $k(\lambda)$ in Table 7, found at Dome C and South Pole throughout the year, is that temperature increases dramatically from local winter to summer throughout the stratosphere, which contributes about 26% to the whole columnar value of ROD($\lambda$). The magnitude of annual stratospheric temperature variations is twice as large at the coastal sites of Antarctica and 1.8 times greater over the Antarctic Plateau than in the Arctic. The intense warming of the stratosphere from winter to summer causes a marked decrease in the number density of air molecules at all stratospheric levels. Thus, as evidenced in Figure 7, the volume Rayleigh-scattering coefficient per unit air pressure $b(\lambda)$ diminishes in the stratosphere when passing from winter to summer by as much as 25% in Antarctica, while the relative decrease at the Arctic sites is only about 13%. This phenomenon underlies the gradual changes in ROD($\lambda$), particularly marked at the Antarctic Plateau sites, and is responsible for the gradual decrease in ROD($\lambda$) associated with variations in $T_o$ observed at Dome C and South Pole over the annual cycle. This leads to negative values of $k(\lambda)$ in Figure 12, with regression coefficients equal to −0.30 at Dome C and −0.61 at South Pole. At McMurdo, the tropospheric contribution to ROD($\lambda$) is more important than at the Antarctic Plateau sites and, hence, the stratospheric warming effects occurring in summer are relatively less important. Thus, because of the more marked predominance of the tropospheric contribution over the stratospheric one, a positive value of $k(\lambda)$ was found, with a regression coeffi-
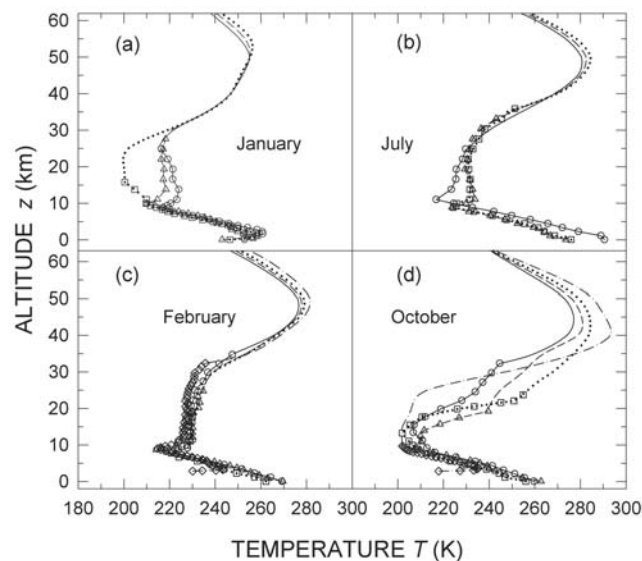
**Figure 10.** (top) January and July CIRA monthly mean profiles of $T(z)$ at 70°N (solid curve), 75°N (dashed curve) and 80°N (dotted curve) latitudes, in the altitude range from the surface level to 60 km, compared with the vertical profiles of $T(z)$ given by some radiosoundings performed in (a) January and (b) July at YCB Cambridge Bay (~70°N) (circles) on 9 January 2002 and 31 July 2003, Resolute (~75°N) (triangles) on 31 January 2003 and 12 July 2002, and Eureka (~80°N) (squares) on 2 January 2000 and 7 July 2001. (bottom) As in Figures 10a and 10b but for the February and October CIRA monthly mean profiles of $T(z)$ at 70°S (solid curve), 75°S (dashed curve), 80°S (dotted curve), and 90°S (dashed and dotted curve) latitudes compared with the vertical profiles of $T(z)$ given by some radiosoundings performed in (c) February and (d) October at Neumayer (~70°S) (circles) on 7 February 2001 and 10 October 2002, Mario Zucchelli (~75°S) (triangles) on 5 February 2000 and 22 October 2003, McMurdo (~80°S) (squares) on 13 February 2003 and 13 October 2003, and South Pole (90°S) (diamonds) on 28 February 2002 and 18 October 2001.

cient of +0.45. The calculations of $k(\lambda)$ at the Neumayer (October–March) and Mario Zucchelli (October–February) stations were made over two more limited ranges of $T_o$, equal to 35 K and 31 K, respectively (while those at the Antarctic Plateau sites were 57 K at Dome C and 52 K at South Pole) and for stratospheric temperature variations during the austral summer of no more than 22–25 K and, hence, for less marked variations in the Rayleigh-scattering contributions given by the stratosphere to ROD($\lambda$). This implies that the Neumayer data plotted in Figure 12 over such a narrow range of $T_o$ provide a negative and relatively low value of $k(\lambda)$, associated with a rather low regression coefficient (equal to −0.25), this result being presumably more due to the large dispersion of data over a very limited range of $T_o$ rather than to the relevance of the stratospheric effects in contrast to the tropospheric ones. Conversely, the positive value of $k(\lambda)$ determined at the Mario Zucchelli station with a regression coefficient of +0.56 agrees very

well with that found at McMurdo, probably owing to the closer dispersion features of its scatterplot to those of McMurdo.

[43] The analysis of the time patterns of pressure and temperature at ground level and 5, 10, and 20 km altitudes, made in sections 4.1 and 4.2, respectively, suggests that surface pressure $p_o$ and temperature $T_o$ can conveniently be used to evaluate the dependence of ROD($\lambda$) on these variables because the vertical profiles of both quantities vary seasonally at all the Arctic and Antarctic sites. On the basis of the results shown in Figure 12 and slope coefficients $k(\lambda)$ given in Table 7, the values of ROD($\lambda$) (in Table 5) can be used to parameterize ROD as a function of measured surface air pressure $p_o$ and temperature $T_o$ observed at the respective stations. The algorithm assumes the following form:

$$\mathrm{ROD}(\lambda, p_o, T_o) = \mathrm{ROD}(\lambda, p_a T_a)(p_o/p_a)[1 + k(\lambda)(T_a - T_o)], \tag{3}$$

where ROD($\lambda$, $p_a$, $T_a$) is the Rayleigh-scattering optical depth calculated at wavelength $\lambda$ for sites listed in Table 5 for the average values of $p_a$ and $T_a$ given in Table 4; $p_o$ is the ground-level air pressure; $T_o$ is the ground-level air temperature; and $k(\lambda)$ is the relative coefficient defining the linear temperature dependence of ROD($\lambda$) on surface temperature $T_o$, as given in Table 7.

[44] For example, to calculate a value of ROD($\lambda$) at wavelength $\lambda$ = 0.55 $\mu$m, for $p_o$ = 975.0 hPa and $T_o$ = 280.0 K, relative to McMurdo station, one makes use of the value of ROD(0.55 $\mu$m, 988.8 hPa, 256.3 K) = 0.09471 found in Table 5 corresponding to the values of $p_a$ and $T_a$ given in Table 4. Coefficient $k$(0.55 $\mu$m) in equation (3) is taken from Table 7, interpolated linearly between values of $k(\lambda)$ given at 0.50 and 1.00 $\mu$m, i.e., $k$(0.55 $\mu$m) = 6.6745 × $10^{-5}$ K$^{-1}$. The value of ROD(0.55 $\mu$m, 988.8 hPa, 256.3 K) is multiplied by the ratio $p_o/p_a$ = 975.0/988.8 = 0.9860 taking into account the surface pressure effect and then by the term in the square brackets in equation (3): in this case, $[1 + 6.6745 \, 10^{-5} \, (256.3 - 280.0)] = 0.9984$, which differs by 1.58% from the corresponding value given in Table 5.

[45] The data given in Table 4 indicate that the ground-level pressure $p_o$ varies during the year by about 6% in the Arctic and at the Antarctic coastal sites, and by ≤8% over the Antarctic Plateau, leading to comparable variations in ROD($\lambda$). Temperature $T_o$ varies within ±15% of the average $T_a$ at the Arctic sites and within ±14% in the Antarctic. If one combines variations of $T_o$ and $k(\lambda)$ from Table 7, corrections in ROD can be made using equation (3) obtaining overall relative variations of +0.08% at 70°N, +0.05% at 75°N, +0.07% at 80°N, −0.06% at 70°S, +0.29% at 75°S and 80°S, and −0.38% at Dome C, and −0.69% at South Pole. Thus, relative to the overall scatter evident in Figure 12, these temperature corrections explain only limited fractions of the day-to-day and seasonal variations in ROD changes equal to 10–25% at the Arctic sites, 20–60% at the Antarctic coastal sites, and 40–50% at Dome C and South Pole.

[46] The percentage errors associated with the day-to-day and season-to-season changes in the vertical profiles of pressure and temperature (as shown in Figures 3 and 4,
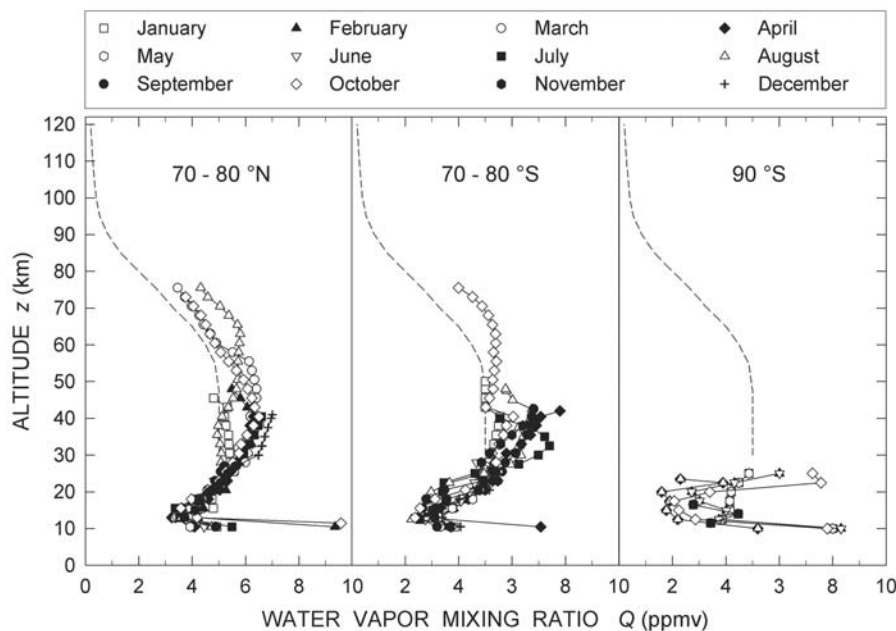
**Figure 11.** (left) Monthly mean vertical profiles of stratospheric water vapor mixing ratio $Q(z)$ as obtained in the latitude range from 70°N to 80°N by averaging the monthly data derived at stratospheric altitudes from various sets of satellite measurements [*Russell et al.*, 1984; *Harries et al.*, 1996; *Randel et al.*, 2001; *Lahoz et al.*, 1996; *Chiou et al.*, 1997; *Peter*, 1998], compared with the vertical profile of $Q(z)$ (dashed curve) defined in the subarctic winter and summer standard atmosphere models [*Anderson et al.*, 1986]. (middle) As in the left plot but for the 70°S−80°S latitude range and for various sets of satellite data [*Russell et al.*, 1984; *Harries et al.*, 1996; *Randel et al.*, 2001; *Lahoz et al.*, 1996; *Chiou et al.*, 1997; *Müller et al.*, 2003a, 2003b; *Morrey and Harwood*, 1998]. (right) As in the left plot but for the 90°S latitude (South Pole) for various sets of satellite and lidar data [*Rosen et al.*, 1991; *Fiocco et al.*, 1996; *Cacciani et al.*, 1997].

respectively, for pairs of monthly data sets taken in January and July at Arctic and Antarctic sites) can be estimated as differences between the overall variability of ROD($\lambda$) and the variability range shown by the values evaluated using equation (3) at respective sites. These differences give a measure of uncertainty (at the $3\sigma$ level) attributable to day-to-day and seasonal variations in profiles of pressure and temperature. The expected relative errors in ROD(0.50 $\mu$m), after equation (3) is applied, are as follows.

[47] 1. In the Arctic, the relative error is ±0.3% to ±0.5%. These evaluations lead to corresponding uncertainties in ROD(0.50 $\mu$m) ranging between 0.0004 and 0.0007. Clean background values of AOD(0.50 $\mu$m) in the Arctic are typically in the range 0.04–0.10 [*Tomasi et al.*, 2007]; thus errors in ROD(0.50 $\mu$m) can lead to relative errors in AOD(0.50 $\mu$m) varying between less than 1% and 2%.

[48] 2. At Antarctic coastal sites, the relative error is ±0.2% to ±0.5%, leading to corresponding absolute errors of ROD(0.50 $\mu$m) between 0.0003 and 0.0007. For clean background conditions at the coast, AOD(0.50 $\mu$m) ranges between 0.02 and 0.08 [*Tomasi et al.*, 2007]. Thus, errors in ROD(0.50 $\mu$m) can result in relative errors in AOD(0.50 $\mu$m) of between less than 1% and 4%.

[49] 3. On the Antarctic Plateau, the relative error is ±0.6% to ±0.7%, leading to errors in ROD(0.50 $\mu$m) close to 0.0006 for typical background conditions, in which

AOD(0.50 $\mu$m) varies from 0.005 to 0.025 [*Tomasi et al.*, 2007], with relative errors ranging mainly between 3% and 13%. The above analysis demonstrates very clearly that computations of ROD($\lambda$) at high-altitude sites need to be done as accurately as possible in cases where AOD values are lower than 0.01, which are, in practice, comparable with the Sun photometer error in determining AOD, mainly owing to calibration inaccuracies. However, especially for extreme seasonal conditions of the atmosphere, further uncertainties in deriving values of AOD($\lambda$) over the entire range of wavelengths typically measured with the Sun photometers could be avoided by performing more precise calculations of ROD($\lambda$) using the local radiosounding data, together with monthly or seasonal mean atmospheric models at stratospheric levels.

[50] Table 5 lists the mean values of ROD($\lambda$) at 88 wavelengths, selected in regular steps of 0.01 $\mu$m from 0.20 to 0.80 $\mu$m, 0.02 $\mu$m from 0.80 to 1.00 $\mu$m, 0.1 $\mu$m from 1.0 to 2.0 $\mu$m, 0.2 $\mu$m from 2 to 3 $\mu$m, and 0.5 $\mu$m from 3 to 4 $\mu$m. However, the central wavelengths of the interference filters used in the various Sun photometers employed at the polar stations (see Table 8) do not coincide with those listed. The same can be said for retrievals of AOD($\lambda$) using satellite radiances. Channels of many sensors in use are listed in Table 9 which do not necessarily match those listed in Table 5. Thus, values of ROD($\lambda$) suitable for

**Table 5.** Mean Values of Rayleigh-Scattering Optical Depth ROD($\lambda$) at 88 Wavelengths, as Obtained for the Sets of Vertical Profiles of Air Pressure, Temperature, and Moisture, Defined From the 4 Year Radiosounding Data Sets Recorded at the Various Selected Arctic and Antarctic Sites[a]

| Wavelength $\lambda(\mu m)$ | YCB Cambridge Bay ($\sim$70°N) | Resolute, Danmarkshavn ($\sim$75°N) | Eureka, Alert, Ny-Ålesund ($\sim$80°N) | Neumayer ($\sim$70°S) Antarctic Coast | Mario Zucchelli ($\sim$75°S) Antarctic Coast | McMurdo ($\sim$80°S) Antarctic Coast | Dome C ($\sim$75°S) Antarctic Plateau | South Pole (90°S) Antarctic Plateau |
|---|---|---|---|---|---|---|---|---|
| 0.20 | $7.7613 \times 10^{0}$ | $7.7621 \times 10^{0}$ | $7.7710 \times 10^{0}$ | $7.5501 \times 10^{0}$ | $7.5179 \times 10^{0}$ | $7.5790 \times 10^{0}$ | $4.9466 \times 10^{0}$ | $5.2486 \times 10^{0}$ |
| 0.21 | 6.1029 | 6.1036 | 6.1106 | 5.9369 | 5.9117 | 5.9598 | 3.8898 | 4.1273 |
| 0.22 | 4.8850 | 4.8856 | 4.8912 | 4.7522 | 4.7320 | 4.7705 | 3.1136 | 3.3037 |
| 0.23 | 3.9676 | 3.9680 | 3.9726 | 3.8597 | 3.8433 | 3.8746 | 2.5289 | 2.6833 |
| 0.24 | 3.2624 | 3.2628 | 3.2665 | 3.1738 | 3.1603 | 3.1860 | 2.0795 | 2.2064 |
| 0.25 | 2.7113 | 2.7117 | 2.7148 | 2.6377 | 2.6265 | 2.6479 | 1.7282 | 1.8337 |
| 0.26 | 2.2746 | 2.2749 | 2.2775 | 2.2128 | 2.2034 | 2.2214 | 1.4499 | 1.5384 |
| 0.27 | 1.9243 | 1.9245 | 1.9267 | 1.8720 | 1.8640 | 1.8792 | 1.2265 | 1.3014 |
| 0.28 | 1.6401 | 1.6403 | 1.6422 | 1.5956 | 1.5888 | 1.6017 | 1.0454 | 1.1093 |
| 0.29 | 1.4075 | 1.4076 | 1.4092 | 1.3692 | 1.3634 | 1.3745 | $8.9715 \times 10^{-1}$ | $9.5192 \times 10^{-1}$ |
| 0.30 | 1.2153 | 1.2154 | 1.2168 | 1.1823 | 1.1773 | 1.1869 | 7.7466 | 8.2195 |
| 0.31 | 1.0553 | 1.0554 | 1.0567 | 1.0267 | 1.0223 | 1.0306 | 6.7269 | 7.1376 |
| 0.32 | $9.2118 \times 10^{-1}$ | $9.2129 \times 10^{-1}$ | $9.2235 \times 10^{-1}$ | $8.9617 \times 10^{-1}$ | $8.9236 \times 10^{-1}$ | $8.9964 \times 10^{-1}$ | 5.8719 | 6.2303 |
| 0.33 | 8.0796 | 8.0806 | 8.0898 | 7.8602 | 7.8268 | 7.8906 | 5.1502 | 5.4646 |
| 0.34 | 7.1182 | 7.1190 | 7.1272 | 6.9249 | 6.8955 | 6.9517 | 4.5373 | 4.8143 |
| 0.35 | 6.2971 | 6.2979 | 6.3051 | 6.1262 | 6.1001 | 6.1499 | 4.0140 | 4.2590 |
| 0.36 | 5.5924 | 5.5930 | 5.5994 | 5.4405 | 5.4174 | 5.4616 | 3.5647 | 3.7824 |
| 0.37 | 4.9844 | 4.9850 | 4.9907 | 4.8491 | 4.8285 | 4.8679 | 3.1772 | 3.3712 |
| 0.38 | 4.4576 | 4.4582 | 4.4633 | 4.3366 | 4.3182 | 4.3534 | 2.8414 | 3.0149 |
| 0.39 | 3.9992 | 3.9997 | 4.0043 | 3.8907 | 3.8741 | 3.9057 | 2.5492 | 2.7049 |
| 0.40 | 3.5987 | 3.5992 | 3.6033 | 3.5010 | 3.4861 | 3.5146 | 2.2940 | 2.4340 |
| 0.41 | 3.2475 | 3.2479 | 3.2516 | 3.1594 | 3.1459 | 3.1716 | 2.0701 | 2.1965 |
| 0.42 | 2.9384 | 2.9388 | 2.9422 | 2.8587 | 2.8465 | 2.8697 | 1.8731 | 1.9874 |
| 0.43 | 2.6655 | 2.6658 | 2.6689 | 2.5932 | 2.5821 | 2.6032 | 1.6991 | 1.8028 |
| 0.44 | 2.4238 | 2.4241 | 2.4268 | 2.3580 | 2.3479 | 2.3671 | 1.5450 | 1.6393 |
| 0.45 | 2.2090 | 2.2092 | 2.2118 | 2.1490 | 2.1399 | 2.1573 | 1.4081 | 1.4940 |
| 0.46 | 2.0176 | 2.0178 | 2.0202 | 1.9628 | 1.9545 | 1.9704 | 1.2861 | 1.3646 |
| 0.47 | 1.8466 | 1.8468 | 1.8490 | 1.7965 | 1.7889 | 1.8034 | 1.1771 | 1.2490 |
| 0.48 | 1.6935 | 1.6937 | 1.6956 | 1.6475 | 1.6405 | 1.6539 | 1.0795 | 1.1454 |
| 0.49 | 1.5560 | 1.5562 | 1.5579 | 1.5137 | 1.5073 | 1.5196 | $9.9183 \times 10^{-2}$ | 1.0524 |
| 0.50 | 1.4322 | 1.4324 | 1.4340 | 1.3933 | 1.3874 | 1.3987 | 9.1294 | $9.6867 \times 10^{-2}$ |
| 0.51 | 1.3206 | 1.3207 | 1.3222 | 1.2847 | 1.2792 | 1.2897 | 8.4177 | 8.9316 |
| 0.52 | 1.2196 | 1.2198 | 1.2212 | 1.1865 | 1.1815 | 1.1911 | 7.7744 | 8.2490 |
| 0.53 | 1.1282 | 1.1283 | 1.1296 | 1.0976 | 1.0929 | 1.1018 | 7.1916 | 7.6306 |
| 0.54 | 1.0452 | 1.0454 | 1.0466 | 1.0169 | 1.0125 | 1.0208 | 6.6627 | 7.0694 |
| 0.55 | $9.6977 \times 10^{-2}$ | $9.6989 \times 10^{-2}$ | $9.7100 \times 10^{-2}$ | $9.4345 \times 10^{-2}$ | $9.3943 \times 10^{-2}$ | $9.4710 \times 10^{-2}$ | 6.1817 | 6.5591 |
| 0.56 | 9.0103 | 9.0113 | 9.0217 | 8.7657 | 8.7284 | 8.7996 | 5.7435 | 6.0941 |
| 0.57 | 8.3829 | 8.3839 | 8.3935 | 8.1554 | 8.1207 | 8.1869 | 5.3436 | 5.6698 |
| 0.58 | 7.8094 | 7.8103 | 7.8193 | 7.5974 | 7.5651 | 7.6268 | 4.9780 | 5.2819 |
| 0.59 | 7.2843 | 7.2851 | 7.2935 | 7.0865 | 7.0564 | 7.1140 | 4.6433 | 4.9267 |
| 0.60 | 6.8027 | 6.8035 | 6.8113 | 6.6180 | 6.5899 | 6.6437 | 4.3363 | 4.6010 |
| 0.61 | 6.3604 | 6.3612 | 6.3685 | 6.1878 | 6.1614 | 6.2117 | 4.0544 | 4.3019 |
| 0.62 | 5.9536 | 5.9543 | 5.9611 | 5.7920 | 5.7674 | 5.8144 | 3.7950 | 4.0267 |
| 0.63 | 5.5789 | 5.5795 | 5.5859 | 5.4274 | 5.4044 | 5.4485 | 3.5562 | 3.7733 |
| 0.64 | 5.2333 | 5.2339 | 5.2399 | 5.0912 | 5.0696 | 5.1109 | 3.3359 | 3.5395 |
| 0.65 | 4.9141 | 4.9147 | 4.9203 | 4.7807 | 4.7604 | 4.7992 | 3.1324 | 3.3237 |
| 0.66 | 4.6190 | 4.6195 | 4.6248 | 4.4936 | 4.4745 | 4.5110 | 2.9443 | 3.1240 |
| 0.67 | 4.3457 | 4.3462 | 4.3512 | 4.2278 | 4.2098 | 4.2441 | 2.7701 | 2.9392 |
| 0.68 | 4.0924 | 4.0929 | 4.0976 | 3.9813 | 3.9644 | 3.9968 | 2.6087 | 2.7679 |
| 0.69 | 3.8574 | 3.8578 | 3.8622 | 3.7527 | 3.7367 | 3.7672 | 2.4588 | 2.6089 |
| 0.70 | 3.6390 | 3.6394 | 3.6436 | 3.5402 | 3.5252 | 3.5539 | 2.3196 | 2.4612 |
| 0.71 | 3.4359 | 3.4363 | 3.4402 | 3.3426 | 3.3284 | 3.3556 | 2.1902 | 2.3239 |
| 0.72 | 3.2468 | 3.2472 | 3.2509 | 3.1586 | 3.1452 | 3.1709 | 2.0696 | 2.1960 |
| 0.73 | 3.0705 | 3.0709 | 3.0744 | 2.9872 | 2.9745 | 2.9988 | 1.9573 | 2.0768 |
| 0.74 | 2.9061 | 2.9065 | 2.9098 | 2.8272 | 2.8152 | 2.8382 | 1.8525 | 1.9656 |
| 0.75 | 2.7526 | 2.7529 | 2.7561 | 2.6779 | 2.6665 | 2.6882 | 1.7546 | 1.8617 |
| 0.76 | 2.6091 | 2.6094 | 2.6124 | 2.5383 | 2.5275 | 2.5481 | 1.6631 | 1.7647 |
| 0.77 | 2.4748 | 2.4751 | 2.4780 | 2.4077 | 2.3974 | 2.4170 | 1.5776 | 1.6739 |
| 0.78 | 2.3491 | 2.3494 | 2.3521 | 2.2854 | 2.2756 | 2.2942 | 1.4974 | 1.5888 |
| 0.79 | 2.2313 | 2.2316 | 2.2341 | 2.1707 | 2.1615 | 2.1791 | 1.4223 | 1.5091 |
| 0.80 | 2.1208 | 2.1210 | 2.1235 | 2.0632 | 2.0544 | 2.0712 | 1.3519 | 1.4344 |
| 0.82 | 1.9196 | 1.9198 | 1.9220 | 1.8675 | 1.8595 | 1.8747 | 1.2236 | 1.2983 |
| 0.84 | 1.7417 | 1.7419 | 1.7439 | 1.6945 | 1.6872 | 1.7010 | 1.1102 | 1.1780 |
| 0.86 | 1.5840 | 1.5842 | 1.5860 | 1.5410 | 1.5345 | 1.5470 | 1.0097 | 1.0714 |
| 0.88 | 1.4438 | 1.4440 | 1.4456 | 1.4046 | 1.3986 | 1.4101 | $9.2034 \times 10^{-3}$ | $9.7653 \times 10^{-3}$ |
| 0.90 | 1.3188 | 1.3189 | 1.3205 | 1.2830 | 1.2775 | 1.2880 | 8.4065 | 8.9197 |
| 0.92 | 1.2070 | 1.2072 | 1.2086 | 1.1743 | 1.1693 | 1.1788 | 7.6941 | 8.1638 |

**Table 5.** (continued)

| Wavelength $\lambda(\mu m)$ | YCB Cambridge Bay ($\sim$70°N) | Resolute, Danmarkshavn ($\sim$75°N) | Eureka, Alert, Ny-Ålesund ($\sim$80°N) | Neumayer ($\sim$70°S) Antarctic Coast | Mario Zucchelli ($\sim$75°S) Antarctic Coast | McMurdo ($\sim$80°S) Antarctic Coast | Dome C ($\sim$75°S) Antarctic Plateau | South Pole (90°S) Antarctic Plateau |
|---|---|---|---|---|---|---|---|---|
| 0.94 | 1.1069 | 1.1070 | 1.1083 | 1.0768 | 1.0722 | 1.0810 | 7.0557 | 7.4864 |
| 0.96 | 1.0169 | 1.0170 | 1.0182 | $9.8931 \times 10^{-3}$ | $9.8510 \times 10^{-3}$ | $9.9314 \times 10^{-3}$ | 6.4822 | 6.8779 |
| 0.98 | $9.3591 \times 10^{-3}$ | $9.3602 \times 10^{-3}$ | $9.3709 \times 10^{-3}$ | 9.1051 | 9.0664 | 9.1403 | 5.9659 | 6.3301 |
| 1.00 | 8.6283 | 8.6293 | 8.6392 | 8.3941 | 8.3584 | 8.4266 | 5.5000 | 5.8358 |
| 1.10 | 5.8810 | 5.8817 | 5.8885 | 5.7214 | 5.6971 | 5.7436 | 3.7488 | 3.9777 |
| 1.20 | 4.1459 | 4.1464 | 4.1511 | 4.0334 | 4.0162 | 4.0490 | 2.6428 | 2.8041 |
| 1.30 | 3.0063 | 3.0067 | 3.0101 | 2.9247 | 2.9123 | 2.9361 | 1.9164 | 2.0334 |
| 1.40 | 2.2329 | 2.2332 | 2.2358 | 2.1723 | 2.1631 | 2.1808 | 1.4234 | 1.5103 |
| 1.50 | 1.6931 | 1.6933 | 1.6953 | 1.6472 | 1.6402 | 1.6535 | 1.0793 | 1.1452 |
| 1.60 | 1.3071 | 1.3072 | 1.3087 | 1.2716 | 1.2662 | 1.2765 | $8.3318 \times 10^{-4}$ | $8.8404 \times 10^{-4}$ |
| 1.70 | 1.0251 | 1.0252 | 1.0264 | $9.9724 \times 10^{-4}$ | $9.9300 \times 10^{-4}$ | 1.0011 | 6.5342 | 6.9331 |
| 1.80 | $8.1520 \times 10^{-4}$ | $8.1530 \times 10^{-4}$ | $8.1623 \times 10^{-4}$ | 7.9308 | 7.8970 | $7.9615 \times 10^{-4}$ | 5.1965 | 5.5137 |
| 1.90 | 6.5641 | 6.5649 | 6.5725 | 6.3860 | 6.3588 | 6.4107 | 4.1843 | 4.4397 |
| 2.00 | 5.3448 | 5.3455 | 5.3516 | 5.1998 | 5.1777 | 5.2199 | 3.4070 | 3.6150 |
| 2.20 | 3.6487 | 3.6492 | 3.6533 | 3.5497 | 3.5346 | 3.5634 | 2.3259 | 2.4678 |
| 2.40 | 2.5752 | 2.5755 | 2.5785 | 2.5053 | 2.4947 | 2.5151 | 1.6416 | 1.7418 |
| 2.60 | 1.8691 | 1.8693 | 1.8715 | 1.8184 | 1.8107 | 1.8254 | 1.1915 | 1.2642 |
| 2.80 | 1.3893 | 1.3895 | 1.3911 | 1.3516 | 1.3458 | 1.3568 | $8.8560 \times 10^{-5}$ | $9.3966 \times 10^{-5}$ |
| 3.00 | 1.0540 | 1.0542 | 1.0554 | 1.0254 | 1.0211 | 1.0294 | 6.7189 | 7.1291 |
| 3.50 | $5.6875 \times 10^{-5}$ | $5.6882 \times 10^{-5}$ | $5.6947 \times 10^{-5}$ | $5.5331 \times 10^{-5}$ | $5.5096 \times 10^{-5}$ | $5.5546 \times 10^{-5}$ | 3.6255 | 3.8468 |
| 4.00 | 3.3331 | 3.3335 | 3.3374 | 3.2427 | 3.2289 | 3.2552 | 2.1247 | 2.2544 |

[a]The values of ROD($\lambda$) are associated with the 4 year average values of surface pressure $p_a$ and temperature $T_a$ given in Table 4.

Sun photometer applications or satellite retrievals must be estimated using an interpolation scheme. This can be implemented using the listing of ROD($\lambda$) given in Table 5.

[51] For example, for wavelength $\lambda_s$ between two consecutive wavelengths $\lambda_j$ and $\lambda_{j+1}$ listed in Table 5, ROD($\lambda_s$) can be calculated through bilogarithmic interpolation in $\lambda_s$ between the values of ROD($\lambda_j$) and ROD($\lambda_{j+1}$) and wavelengths $\lambda_j$ and $\lambda_{j+1}$. The inverse power law was shown in Figure 1 and defined in equation (1). Several tests validate this bilogarithmic interpolation procedure, made on the basis of the classification of sites listed in Table 4 for wavelengths selected in Table 7. Values of ROD($\lambda_s$)$_{int}$ obtained through interpolation were compared with the corresponding values of ROD($\lambda_s$)$_{calc}$, calculated using the atmospheric models defined for each site using the radiosoundings. The values of ratio $\Re(\lambda_s)$ between ROD($\lambda_s$)$_{int}$

and ROD($\lambda_s$)$_{calc}$ obtained at the nine selected wavelengths $\lambda_s$ are given in Table 10. Extreme values of $\Re(\lambda_s)$ are 1.00103 at 0.205 $\mu$m at South Pole and 0.99998 at 0.810 $\mu$m wavelength at Mario Zucchelli station. In general, $\Re(\lambda_s)$ is within ±0.03% of unity, evidence that the interpolation scheme works very well. In addition, Table 10 lists average values and standard deviations of $\varepsilon(\lambda_s)$ obtained for the stations at selected wavelengths, within the respective intervals $\lambda_j$ and $\lambda_{j+1}$ from Table 5.

## 7. Calculation of the Volume Rayleigh-Scattering Coefficient at Lidar Wavelengths

[52] The calculations of volume Rayleigh-scattering coefficient $\beta(\lambda)$ made in section 2.2 for different conditions of air pressure and temperature can also be used in the analysis

**Table 6.** Ratios Between the Mean Values of Rayleigh-Scattering Optical Depth ROD(0.50 $\mu$m) Normalized to the Surface Level Pressure $p_s$ = 1013.25 hPa and the Values of ROD(0.50 $\mu$m) Calculated for $p_s$ = 1013.25 hPa by *Bucholtz* [1995], *Bodhaine et al.* [1999], and *Tomasi et al.* [2005] Using the 45°N and 60°N Atmospheric Models of *Anderson et al.* [1986][a]

| Authors and Atmospheric Model | YCB Cambridge Bay ($\sim$70°N) | Resolute, Danmarkshavn ($\sim$75°N) | Eureka, Alert, Ny-Ålesund ($\sim$80°N) | Neumayer ($\sim$70°S) Antarctic Coast | Mario Zucchelli ($\sim$75°S) Antarctic Coast | McMurdo ($\sim$80°S) Antarctic Coast | Dome C ($\sim$75°S) Antarctic Plateau | South Pole (90°S) Antarctic Plateau |
|---|---|---|---|---|---|---|---|---|
| *Bucholtz* [1995], subarctic summer | 1.0014 | 1.0048 | 1.0048 | 1.0020 | 1.0012 | 1.0023 | 1.0039 | 1.0042 |
| *Bucholtz* [1995], subarctic winter | 0.9986 | 1.0020 | 1.0020 | 0.9992 | 0.9984 | 0.9995 | 1.0011 | 1.0014 |
| *Bodhaine et al.* [1999], sea level 45°N | 0.9989 | 1.0023 | 1.0022 | 0.9994 | 0.9987 | 0.9998 | 1.0013 | 1.0017 |
| *Tomasi et al.* [2005], subarctic summer | 1.0030 | 1.0064 | 1.0064 | 1.0036 | 1.0028 | 1.0039 | 1.0055 | 1.0058 |
| *Tomasi et al.* [2005], subarctic winter | 0.9994 | 1.0029 | 1.0028 | 1.0000 | 0.9992 | 1.0004 | 1.0019 | 1.0022 |

[a]Mean values of Rayleigh-scattering optical depth ROD(0.50 $\mu$m) are given in Table 5 after normalization to the value of surface level pressure $p_s$ given in Table 4 for each of the eight latitude/altitude height classes.
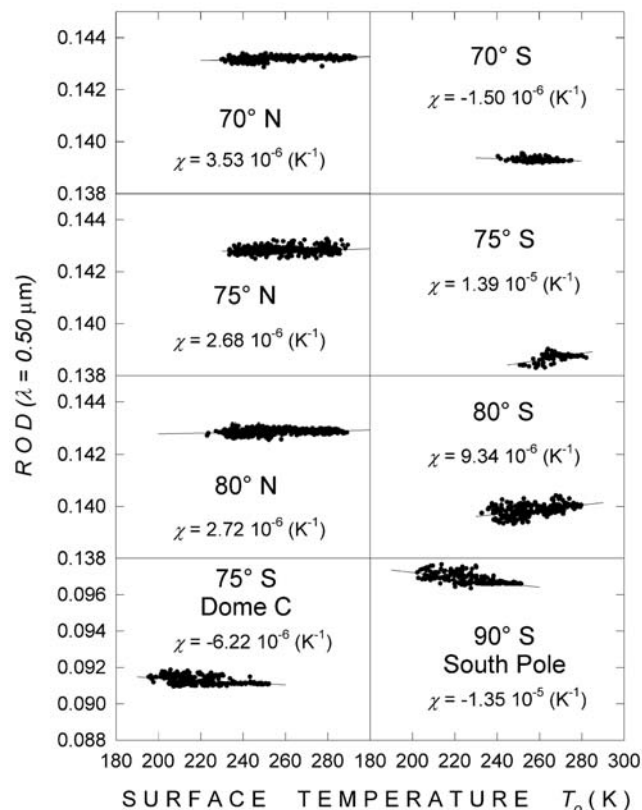
**Figure 12.** Plots of the Rayleigh-scattering optical depth ROD calculated at the 0.50 $\mu$m wavelength and normalized to the average surface-level pressure $p_a$ as a function of surface temperature $T_o$, obtained for the eight sets of vertical profiles of $p(z)$, $T(z)$, and RH($z$) over the altitude range from surface level to 120 km. The profiles were determined from the radiosounding data sets, completed with the CIRA monthly mean profiles of $p(z)$ and $T(z)$, and those of water vapor mixing ratio $Q(z)$ derived from satellite data. The data are shown separately for each of the following site classes: 70°N (YCB Cambridge Bay), 75°N (Resolute, Danmarkshavn), 80°N (Eureka, Alert and Ny-Ålesund), 70°S (Neumayer), 75°S (Mario Zucchelli), 80°S (McMurdo), Antarctic Plateau 75°S (Dome C), and Antarctic Plateau 90°S (South Pole).

of lidar measurements made at polar stations, namely Ny Ålesund, ALOMAR Observatory, Barrow, and Eureka in the Arctic and Dumont D'Urville, Syowa, Davis, McMurdo, Dome C, and South Pole in Antarctica. Table 11 lists these sites along with descriptions and wavelengths of lidar systems currently in use. Respective values of $\beta(\lambda)$ are in Table 12 for standard surface conditions, $p_s = 1013.25$ hPa and air temperature $T_s = 273$ K. These values vary with altitude for differing profiles of $p(z)$ and $T(z)$ and to a lesser extent on water vapor partial pressure $e(z)$ and $CO_2$ concentration $C(z)$ [*Tomasi et al.*, 2005]. In reality, $\beta(\lambda)$ at each altitude is equal to the product of molecular number density $N(z)$ and the Rayleigh-scattering cross section $\sigma(\lambda, z)$, where $N(z)$ depends on ambient pressure and temperature, proportional to the ratio $p(z)/p_s$ and inversely proportional to the ratio $T(z)/T_s$ [*Penndorf*, 1957; *Bodhaine et al.*, 1999]. The Rayleigh-scattering cross section $\sigma(\lambda, z)$ per molecule for incident unpolarized radiation depends not only on $p(z)$ and $T(z)$ but also on the refractive index $n(\lambda, z)$ of air and *King* [1923] factor $F(\lambda, z)$ for the depolarization of air.

[53] It is obvious from this brief account that functions describing the variations in $\beta(\lambda, z)$ can be very complicated and are therefore normally evaluated only for standard atmospheric models [*Anderson et al.*, 1986]. In polar atmospheres, $\beta(\lambda, z)$ decreases as a function of altitude with features similar to those shown in Figure 2. On this point, Figure 13 illustrates the dependence of $\beta(0.523 \mu m)$ on air pressure $p$ and temperature $T$ for constant values of partial pressure $e$ and concentration $C$. The relationships are nearly linear with air pressure and decreases in an exponential fashion with increasing temperature.

[54] As was noted in reference to Figure 5, $\beta(\lambda, z)$ varies significantly with altitude in the polar atmosphere, depending on seasonal profiles of $p(z)$ and $T(z)$. In this regard, it is illuminating to examine the vertical profiles of ratio $\beta(\lambda, z)/p(z)$ shown in Figure 6, which presents results for January and July conditions at Alert and South Pole to emphasize the strong dependence of $\beta(\lambda, z)$ on the thermal structure of the atmosphere. It is clear that the best approach for examining lidar data is to account for the vertical profiles of $\beta(\lambda, z)$ as a function of $p(z)$, $T(z)$, and $e(z)$ measured locally using radiosondes. Table 12 lists the monochromatic values of Rayleigh-scattering cross section $\sigma(\lambda)$ at the lidar wavelengths given in Table 11. This parameter varies as a

**Table 7.** Mean Values of Relative Slope Coefficient $k(\lambda)$ Obtained at Various Wavelengths and for the Eight Latitude/Altitude Site Classes to Define the Dependence of ROD($\lambda$) on Surface Temperature Conditions[a]

| Wavelength ($\mu$m) | YCB Cambridge Bay (~70°N) | Resolute, Danmarkshavn (~75°N) | Eureka, Alert, Ny-Ålesund (~80°N) | Neumayer (~70°S) Antarctic Coast | Mario Zucchelli (~75°S) Antarctic Coast | McMurdo (~80°S) Antarctic Coast | Dome C (~75°S) Antarctic Plateau | South Pole (90°S) Antarctic Plateau |
|---|---|---|---|---|---|---|---|---|
| 0.20 | $2.4659 \times 10^{-5}$ | $1.8792 \times 10^{-5}$ | $1.9015 \times 10^{-5}$ | $-1.0767 \times 10^{-5}$ | $1.0045 \times 10^{-4}$ | $6.6763 \times 10^{-5}$ | $-6.8106 \times 10^{-5}$ | $-1.3931 \times 10^{-4}$ |
| 0.25 | $2.4655 \times 10^{-5}$ | $1.8787 \times 10^{-5}$ | $1.9011 \times 10^{-5}$ | $-1.0770 \times 10^{-5}$ | $1.0044 \times 10^{-4}$ | $6.6754 \times 10^{-5}$ | $-6.8108 \times 10^{-5}$ | $-1.3932 \times 10^{-4}$ |
| 0.30 | $2.4653 \times 10^{-5}$ | $1.8785 \times 10^{-5}$ | $1.9008 \times 10^{-5}$ | $-1.0771 \times 10^{-5}$ | $1.0044 \times 10^{-4}$ | $6.6750 \times 10^{-5}$ | $-6.8109 \times 10^{-5}$ | $-1.3932 \times 10^{-4}$ |
| 0.50 | $2.4651 \times 10^{-5}$ | $1.8782 \times 10^{-5}$ | $1.9005 \times 10^{-5}$ | $-1.0772 \times 10^{-5}$ | $1.0043 \times 10^{-4}$ | $6.6745 \times 10^{-5}$ | $-6.8110 \times 10^{-5}$ | $-1.3932 \times 10^{-4}$ |
| 0.80 | $2.4650 \times 10^{-5}$ | $1.8781 \times 10^{-5}$ | $1.9004 \times 10^{-5}$ | $-1.0772 \times 10^{-5}$ | $1.0043 \times 10^{-4}$ | $6.6743 \times 10^{-5}$ | $-6.8111 \times 10^{-5}$ | $-1.3932 \times 10^{-4}$ |
| 1.00 | $2.4649 \times 10^{-5}$ | $1.8780 \times 10^{-5}$ | $1.9004 \times 10^{-5}$ | $-1.0773 \times 10^{-5}$ | $1.0043 \times 10^{-4}$ | $6.6743 \times 10^{-5}$ | $-6.8111 \times 10^{-5}$ | $-1.3932 \times 10^{-4}$ |
| 2.00 | $2.4649 \times 10^{-5}$ | $1.8780 \times 10^{-5}$ | $1.9003 \times 10^{-5}$ | $-1.0773 \times 10^{-5}$ | $1.0043 \times 10^{-4}$ | $6.6742 \times 10^{-5}$ | $-6.8111 \times 10^{-5}$ | $-1.3932 \times 10^{-4}$ |
| 3.00 | $2.4649 \times 10^{-5}$ | $1.8780 \times 10^{-5}$ | $1.9003 \times 10^{-5}$ | $-1.0773 \times 10^{-5}$ | $1.0043 \times 10^{-4}$ | $6.6742 \times 10^{-5}$ | $-6.8111 \times 10^{-5}$ | $-1.3932 \times 10^{-4}$ |
| 4.00 | $2.4649 \times 10^{-5}$ | $1.8780 \times 10^{-5}$ | $1.9003 \times 10^{-5}$ | $-1.0773 \times 10^{-5}$ | $1.0043 \times 10^{-4}$ | $6.6742 \times 10^{-5}$ | $-6.8111 \times 10^{-5}$ | $-1.3932 \times 10^{-4}$ |

[a]Measured in $K^{-1}$.

**Table 8.** Research Groups and Measurement Sites of the POLAR-AOD Network, With Sun Photometers Used at Arctic and Antarctic Sites and the Respective Central Wavelengths $\lambda_p$ of the Narrowband Interference Filters Mounted on the Instruments

| Research Groups | Arctic and Antarctic Measurement Sites | Sun Photometer Models | List of Central Wavelengths $\lambda_p$ (nm) |
|---|---|---|---|
| ISAC-CNR (Italy) | Terra Nova Bay "Mario Zucchelli" station (74°42'S, 164°07'E, 15 m above MSL), | UVISIR-2 [De Santis et al., 1994] | 320.2, 335.3, 359.3, 401.3, 459.6, 505.9, 550.0, 671.3, 780.0, 865.2, 939.0, 1047.4 |
| | Dome C (75°06'S, 123°21'E, 3233 m above MSL), | FISBAT [Tomasi et al., 1983] | 400.6, 441.5, 509.1, 549.8, 669.7, 879.5, 947.3, 1040.8 |
| | Ny Ålesund "Dirigibile Italia" station (78°54'N, 11°53'E, 2 m above MSL) | ASP-15WL [Tomasi et al., 2000] | 320.9, 343.5, 369.0, 380.5, 413.0, 450.1, 500.2, 550.0, 610.1, 675.8, 778.8, 817.5, 863.0, 945.0, 1025.0 |
| | | PREDE POM 01 [Di Carmine et al., 2005] | 400, 500, 870, and 1020 |
| AWI (Germany) | Ny Ålesund «AWIPEV station» (78°54'N, 11°53'E, 2 m above MSL), | SP1A [Herber et al., 2002] | 375, 371, 380, 416, 443, 500, 532, 609, 675, 778, 864, 911, 947, 961, 1025, 1046, 1062 |
| | Neumayer (70°38'S, 8°15'W, 40 m above MSL) | SP2H [Herber et al., 2002] | 367, 380, 413, 441, 501, 531, 605, 673, 776, 862, 912, 949, 1023, 1045 |
| | | STAR01 [Herber et al., 2002] | 390, 441, 501, 531, 605, 673, 776, 862, 949, 1045 |
| GMD/NOAA (USA) | Barrow (71°19'N, 156°36'W, 8 m above MSL), | SP01-A [Stone, 2002] | 413, 500, 675, 865. |
| | Alert (82°28'N, 62°30'W, 210 m above MSL), | SP02 [Stone, 2002] | 411, 500, 675, 862 (or 368, 610, 778, 1020) |
| | South Pole (90°00'S, 139°16'E, 2841 m above MSL) | | |
| NIPR (Japan) | Ny Ålesund Rabben station (78° 54'N, 11° 53'E, 12 m above MSL), | PREDE POM 02L [Aoki and Fujiyoshi, 2003] | 315, 340, 380,400, 500, 675, 870, 940, 1020, 1600, 2200 |
| | Syowa (69°00'S, 39°35'E, 29 m above MSL) | | |
| AARI (Russia) | Tiksi (71°35'N, 128°47'E, 40 m above MSL), | SP-6 and SP-7 [Radionov and Marshunova, 1992; Radionov, 2005] | 395, 408, 479, 581, 651, 789, 873, 1041. |
| | Mirny (66°33'S, 93°01'E, 40 m above MSL) | | |
| PMOD/WRC (Switzerland) | Summit (72°20'N, 38°45'W, 3270 m above MSL), | PFR (Precision Filter Radiometer) [Wehrli, 2005] | 368, 412, 500, 862 |
| FMI (Finland) | Sodankilä (67°22'N, 26°38'E, 184 m above MSL), | PFR (N29 and N32) [Wehrli, 2005] | 367.6, 411.4, 500.5, 861.6 |
| | Marambio (64°14'S, 56°37'W, 205 m above MSL), | Microtop II 92 | 340, 380, 440, 500, 675, 870, 936, 1020 |
| | Aboa (73°03'S, 13°25'W, 400 m above MSL) | | |
| NILU (Norway) | Ny Ålesund "Sverdrup" station (78°58'N, 11°54'E, 474 m above MSL), Troll (72°00'S, 2°32'E, 1298 m above MSL) | PFR (N18) [Wehrli, 2005] | 368, 412, 500, 862 |
| GOA/Valladolid Univ. (Spain), ALOMAR, Andoya Rocket Range (Norway) and NILU (Norway) | ALOMAR (69°17'N, 16°00'E, 380 m above MSL) (Norway) | CIMEL CE-318-1 [Holben et al., 1998] | 340, 380, 440, 500, 675, 870, 939, 1020 |
| PAS Oceanology Institute (Poland) | Hornsund (77°00'N, 15°33'E, 10 m above MSL) | Microtop II (Solar Light web); [Ponczkowska et al. [2009] | 340, 380, 440, 500, 675, 870, 936, 1020 |

**Table 9.** List of Central Wavelengths $\lambda_c$ Characterizing the Spectral Channels of the Sensors Mounted On Board Satellites for Polar Observations, Which Could Be Used to Calculate Rayleigh-Scattering Parameters Suitable for Retrieval Procedures of Aerosol Parameters From Polar Satellite Observations[a]

| Sensor/Satellite | Central Wavelengths $\lambda_c$ of the Sensor Channels (nm) | Half-Bandwidth $\Delta\lambda$ (nm) |
|---|---|---|
| TOMS/Earth Probe (and other TOMS/Nimbus-7 algorithm versions for UV Absorption Index) | 312.3, 317.4, 317.5, 331.0, 331.2, 340, 360, 368, 380 | <1 |
| MODIS/Terra and Aqua | 470, 550, 1240 | 20 |
| | 1640 | 24 |
| | 865 | 35 |
| | 659, 2130 | 50 |
| MISR/Terra | 446, 558, 672, 867 | 2.6 |
| AATSR/Envisat | 555, 659, 865 | 20 |
| | 1610 | 60 |
| | 3700 | 380 |
| MERIS/Envisat | 760, 625 | 3.75 |
| | 681.25, 753.75 | 7.5 |
| | 412.5, 442.5, 490, 510, 560, 620, 665, 708.75, 885, 900 | 10 |
| | 778.75 | 15 |
| | 865 | 20 |
| SeaWiFS/SeaStar Spacecraft | 412, 443, 490, 510, 555, 670 | 20 |
| | 765, 865 | 40 |
| POLDER/ADEOS-1 | 444.5,[b] 445.5,[b] 446.0[b] | 19.5 ÷ 20 |
| | 446.0, 496.0, 560.0 | 18.7 ÷ 21.5 |
| | 665.5,[b] 665.2,[b] 666.5[b] | 20.6 ÷ 21.0 |
| | 765.5, 771.5 | 10.4 ÷ 37.4 |
| | 851.0,[b] 853.5,[b] 850.5[b] | 37.4 ÷ 39.2 |
| | 904.0 | 21.2 |
| POLDER/ADEOS-2 | 447.5[b] | 19.2 |
| | 497.0, 495.5, 560.0 | 18.3 ÷ 21.5 |
| | 666.0[b] | 19.0 |
| | 765.0, 769.0 | 10.8 ÷ 37.0 |
| | 851.0[b] | 38.7 |
| | 904 | 20.9 |
| Global Imager (GLI)/ADEOS-2 | 380, 400, 412, 443, 460, 490 | 10 |
| | 520, 545, 565, 625, 666, 678, 680, 710, 749, 763, 865 | 10 |
| | 1050, 1240 | 20 |
| | 1380 | 40 |
| | 545 | 50 |
| | 660 | 60 |
| | 460, 1135 | 70 |
| | 825 | 110 |
| | 1640 | 200 |
| | 2210 | 220 |
| | 3715 | 330 |
| HRV-IR and VEGETATION/SPOT-4 and SPOT-5 | 450 | 20 |
| | 645 | 70 |
| | 545 | 90 |
| | 835 | 110 |
| | 1665 | 170 |
| ETM+/LANDSAT 7 | 660 | 60 |
| | 533 | 65 |
| | 565 | 80 |
| | 825 | 150 |
| | 1650 | 200 |

[a]The values of half-bandwidth $\Delta\lambda$ are given in the third column for the various sensors and channels.
[b]Polarized light channels.

**Table 10.** Average Values of Ratio $\Re(\lambda_s) = ROD(\lambda_s)_{int}/ROD(\lambda_s)_{calc}$ Calculated for the Sets of Atmospheric Profiles Defined for the Eight Latitude/Altitude Site Classes at the Nine Wavelengths $\lambda_s$ Selected Throughout the Spectral Range From 0.20 to 4.0 $\mu$m and Corresponding Average Values of Spectral Exponent $\varepsilon(\lambda_s)$ With Their Standard Deviations

| | Ratio $\Re(\lambda_s) = ROD(\lambda_s)_{int}/ROD(\lambda_s)_{calc}$ | | | | | | | | |
| Wavelength $\lambda_s$ ($\mu$m) | YCB Cambridge Bay ($\sim$70°N) | Resolute, Danmarkshavn ($\sim$75°N) | Eureka, Alert, Ny-Ålesund ($\sim$80°N) | Neumayer ($\sim$70°S) Antarctic Coast | Mario Zucchelli ($\sim$75°S) Antarctic Coast | McMurdo ($\sim$80°S) Antarctic Coast | Dome C ($\sim$75°S) Antarctic Plateau | South Pole (90°S) Antarctic Plateau | Average Spectral Exponent $\varepsilon(\lambda_s)$ |
|---|---|---|---|---|---|---|---|---|---|
| 0.205 | 1.00102 | 1.00102 | 1.00102 | 1.00102 | 1.00102 | 1.00102 | 1.00102 | 1.00103 | $-4.9264 \pm 0.0004$ |
| 0.255 | 1.00023 | 1.00026 | 1.00025 | 1.00024 | 1.00025 | 1.00026 | 1.00025 | 1.00024 | $-4.4779 \pm 0.0006$ |
| 0.305 | 1.00009 | 1.00006 | 1.00010 | 1.00011 | 1.00011 | 1.00009 | 1.00010 | 1.00010 | $-4.3045 \pm 0.0012$ |
| 0.505 | 0.99999 | 1.00002 | 0.99999 | 1.00000 | 0.99999 | 1.00001 | 1.00001 | 1.00001 | $-4.0985 \pm 0.0013$ |
| 0.810 | 1.00001 | 0.99999 | 1.00001 | 1.00001 | 0.99998 | 1.00000 | 1.00001 | 1.00000 | $-4.0369 \pm 0.0007$ |
| 1.050 | 1.00005 | 1.00005 | 1.00005 | 1.00005 | 1.00005 | 1.00005 | 1.00005 | 1.00006 | $-4.0217 \pm 0.0001$ |
| 2.100 | 1.00001 | 1.00002 | 1.00001 | 1.00002 | 1.00002 | 1.00000 | 1.00002 | 1.00000 | $-4.0054 \pm 0.0001$ |
| 3.250 | 1.00000 | 1.00003 | 1.00003 | 0.99999 | 1.00003 | 1.00001 | 1.00002 | 1.00002 | $-4.0022 \pm 0.0002$ |
| 3.750 | 1.00000 | 1.00000 | 1.00001 | 1.00001 | 1.00001 | 1.00001 | 1.00002 | 1.00001 | $-4.0017 \pm 0.0001$ |

function of altitude dependent on $p(z)$, $T(z)$, $e(z)$, and $C(z)$ as described above, noting that the molecular backscattering coefficient $\beta_{BS}(\lambda)$ is proportional to $\sigma(\lambda)$ [*Klett*, 1985; *Cairo et al.*, 1999].

## 8. Conclusions

[55] The analysis of over 2200 radiosoundings representing 11 polar locations (six Arctic and five Antarctic) revealed large seasonal variations in the vertical profiles of both pressure and temperature. Spectral volume Rayleigh-scattering coefficients vary significantly with variable profiles of pressure and temperature, decreasing proportionally with pressure and increasing as temperature decreases with altitude (Figure 2).

[56] As a result of these dependences, $ROD(\lambda)$ also varies appreciably with season at high latitudes. In order to determine $ROD(\lambda)$ accurately, monochromatic values were calculated for the vertical profiles of pressure, temperature, and moisture parameters representing eight polar regions (Table 5) relating to 4 year average values of surface pressure $p_a$ and temperature $T_a$ (Table 4). For each region, the dependence of ROD on pressure and temperature was accounted for by employing a correction algorithm on the basis of equation (3), in which a pressure correction is made in terms of measured and annual average pressure ($p_o/p_a$) and a temperature correction is made in terms of the difference between annual average and measured temperature ($T_a - T_o$) on the basis of a family of spectral slope coefficients $k(\lambda)$ (Table 7). Despite large fluctuations of pressure and temperature through the atmosphere with season and from one day to another, this algorithm was found to produce values of ROD accurate to within $\pm0.08\%$ at the six sea-level Arctic sites, $\pm0.30\%$ at the three Antarctic coastal sites, and $\pm0.70\%$ at the two Antarctic Plateau sites. Although accurate, because background conditions in these regions are so pristine in terms of their turbidity, the values of AOD, derived at visible wavelengths and ranging from as low as 0.002 on the Antarctic Plateau to 0.01 at coastal sites in the Arctic, are still subject to potentially large errors, such as those due to calibration of Sun photometers, which are in general close to 0.01 in the visible. Under these pristine conditions, the relative errors of AOD data due to Rayleigh-scattering optical depth correction range from less than 1% to no more than 2% at the Arctic sites, from less than 1% to 4% at the coastal Antarctic sites, and from 3% to 13% over the Antarctic Plateau. Under more turbid conditions, e.g., when incursions of haze, dust, smoke, sea salt, or volcanic aerosols from low latitudes occur, such errors can be an order of magnitude less. In either case, it is prudent to make the most accurate calculations of Rayleigh scattering when processing polar Sun photometer data to minimize errors, and we propose this methodology to be adopted to achieve this goal.

## Appendix A: Surface-Level Measurements of the Yearly Average Volume Concentration of $CO_2$ at Arctic and Antarctic Sites

[57] In the improved algorithm of *Tomasi et al.* [2005] used to calculate the spectral values of Rayleigh-scattering optical depth ROD at UV to IR wavelengths, for the Arctic and Antarctic stations listed in Table 1, the volume concentration $C(z)$ of carbon dioxide was assumed to be equal to 380 ppmv at all sites, in the whole troposphere, stratosphere, and low mesosphere (up to 75 km altitude), according to the 2007 surface-level measurements of this concentration parameter performed by various institutions at the following seven Arctic and five Antarctic stations: (1) Ocean Station "M" (Norway), by National Oceanic and Atmospheric Administration (NOAA)/Global Monitoring Division (GMD); (2) Ny-Ålesund/Zeppelin (Norway), by NOAA/GMD; (3) Pallas-Sammaltunturi (Finland), by NOAA/GMD; (4) Teriberka (Russia), by the Main Geophysical Observatory (MGO), St. Petersburg, Russia; (5) Barrow (USA), by NOAA/GMD; (6) Alert (Canada), by NOAA/GMD and Commonwealth Scientific and Industrial Research Organisation (CSIRO), Australia; (7) Summit (Greenland, Denmark), by NOAA/GMD; (8) Palmer (USA), by NOAA/GMD; (9) Halley Bay (UK), by NOAA/GMD; (10) Syowa (Japan), by NOAA/GMD and NIPR; (11) Mawson (Australia), by CSIRO; and (12) South Pole (USA), by NOAA/GMD and CSIRO. The yearly and monthly (for January and July only) average values of $CO_2$ volume concentration $C$

**Table 11.** Research Groups, Measurement Sites, and Wavelengths of Some Lidars Used at Arctic and Antarctic Sites

| Research Group | Measurement Site | Lidar | Wavelength (nm) |
|---|---|---|---|
| AWI (Germany) | Ny Ålesund «AWIPEV station» (78°54′N, 11°53′E, 2 m above MSL) | Stratospheric ozone and aerosol lidar [Beyerle et al., 1994; Müller et al., 2003] | 308, 353, 532, 1064 |
| | | Tropospheric lidar | 532, 607 |
| ALOMAR, Andoya Rocket Range (Norway) | ALOMAR Observatory (69°17′N, 16°01′E, 380 m above MSL) | DIAL Rayleigh, Mie, and Raman lidar [Scateboe, 1996] | 308, 353, 532, 1064 |
| | | Sodium lidar [Scateboe, 1996] | 589 |
| | | Tropospheric lidar | 532 |
| GMD/NOAA (USA) | Barrow (71°19′N, 156°36′W, 8 m above MSL) | C lidar [Browell, 1991] | 308, 353 |
| CREST (Canada) PEARL (Canada) | Eureka (80°00′N, 85°49′E, 10 m above MSL) | Raman DIAL lidar [Donovan et al., 1998] | 353, 385 |
| | | MRJ/CRL lidar | 532, 1064 |
| | | Tropospheric lidar | 532 |
| IFAC-CNR (Italy) ENEA/ISAC-CNR (Italy) | Dumont D'Urville (66°40′S, 140°01′E, 15 m above MSL) | Automatic depolarization lidar [Del Guasta et al., 1993] | 355, 532 |
| | | DIAL Rayleigh-Raman Lidar | 308, 353, 355, 532, 608, 1064 |
| Bureau of Meteorology (BoM) (Australia) | Davis (68°35′S, 77°59′E, 15 m above MSL) | Troposheric lidar [Klekociuk et al., 2003] | 532 |
| ENEA/ISAC-CNR (Italy) | McMurdo (77°51′S, 166°40′E, 10 m above MSL) | Rayleigh-Raman lidar [Di Donfrancesco et al., 1996; Adriani et al., 2004] | 532, 608, 1064 |
| | Ny Ålesund «AWIPEV station» (78°54′N, 11°53′E, 2 m above MSL) | Tropospheric lidar | 532 |
| IFAC-CNR (Italy) | Dome C (75°06′S, 123°21′E, 3233 m above MSL) | Automatic depolarization lidar | 532 |
| NASA GSFC (USA) University of Illinois (USA) | South Pole (90°00′S, 139°16′E, 2841 m above MSL) | Micropulse Lidar [Mahesh et al., 2005] | 523, 527 |
| | | Fe/Rayleigh lidar [Pan et al., 2002] | 386, 772 |
| Shinshu University, Nagano, and NIPR (Japan) | Syowa (69°00′S, 39°35′E, 29 m above MSL) | Sodium lidar [Kawahara et al., 2002] | 589 |

**Table 12.** Values of Volume Rayleigh-Scattering Coefficient $\beta(\lambda)$, Cross Section $\sigma(\lambda)$, and Backscattering Coefficient $\beta_{BS}(\lambda)$ Calculated at the 13 Lidar Wavelengths Listed in Table 11[a]

| Wavelength $\lambda$ ($\mu$m) | Coefficient $\beta(\lambda)$ (km$^{-1}$) | Cross Section $\sigma(\lambda)$ (cm$^{-2}$) | Backscattering Coefficient $\beta_{BS}(\lambda)$ (km$^{-1}$ sr$^{-1}$) |
|---|---|---|---|
| 0.308 | $1.3550 \times 10^{-1}$ | $5.0430 \times 10^{-26}$ | $1.6170 \times 10^{-2}$ |
| 0.353 | $7.5850 \times 10^{-2}$ | $2.8230 \times 10^{-26}$ | $9.0540 \times 10^{-3}$ |
| 0.355 | $7.4060 \times 10^{-2}$ | $2.7570 \times 10^{-26}$ | $8.8410 \times 10^{-3}$ |
| 0.385 | $5.2700 \times 10^{-2}$ | $1.9620 \times 10^{-26}$ | $6.2910 \times 10^{-3}$ |
| 0.386 | $5.2130 \times 10^{-2}$ | $1.9400 \times 10^{-26}$ | $6.2230 \times 10^{-3}$ |
| 0.523 | $1.4870 \times 10^{-2}$ | $5.5360 \times 10^{-27}$ | $1.7750 \times 10^{-3}$ |
| 0.527 | $1.4420 \times 10^{-2}$ | $5.3660 \times 10^{-27}$ | $1.7210 \times 10^{-3}$ |
| 0.532 | $1.3870 \times 10^{-2}$ | $5.1630 \times 10^{-27}$ | $1.6560 \times 10^{-3}$ |
| 0.589 | $9.1580 \times 10^{-3}$ | $3.4090 \times 10^{-27}$ | $1.0930 \times 10^{-3}$ |
| 0.607 | $8.1020 \times 10^{-3}$ | $3.0160 \times 10^{-27}$ | $9.6710 \times 10^{-4}$ |
| 0.608 | $8.0480 \times 10^{-3}$ | $2.9960 \times 10^{-27}$ | $9.6070 \times 10^{-4}$ |
| 0.772 | $3.0580 \times 10^{-3}$ | $1.1380 \times 10^{-27}$ | $3.6500 \times 10^{-4}$ |
| 1.064 | $8.3940 \times 10^{-4}$ | $3.1240 \times 10^{-28}$ | $1.0020 \times 10^{-4}$ |

[a]For standard surface conditions of air pressure $p_s = 1013.25$ hPa, air temperature $T_s = 273.16$ K and water vapor partial pressure $e_s = 3.665$ hPa (for RH = 60%).

measured in 2007 at the ground level of the 12 GAW stations are given in Table A1, according to the data of the World Data Center for Greenhouse Gases web page (see http://gaw.kishou.go.jp/wdcgg/).
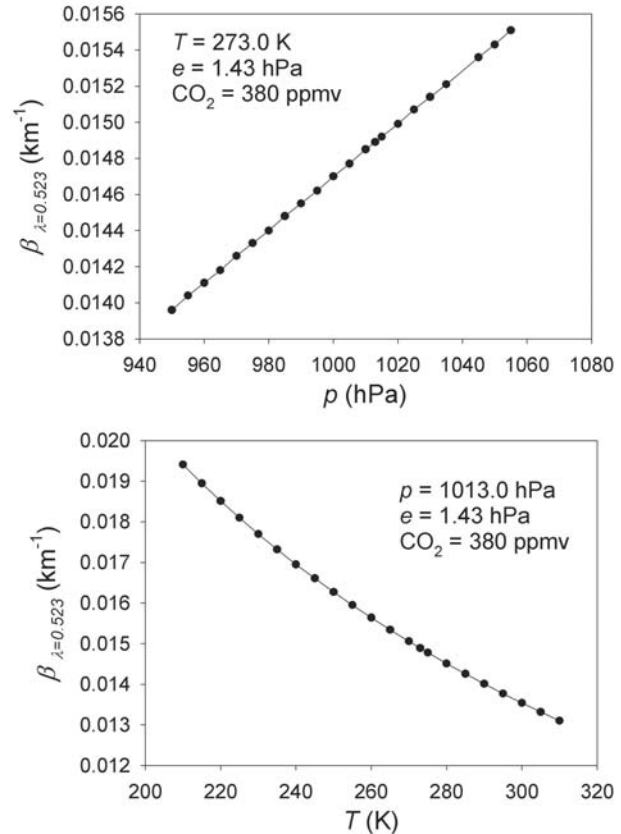


**Figure 13.** (top) Dependence curve of volume Rayleigh-scattering coefficient $\beta(0.523~\mu\text{m})$ on air pressure $p$ for fixed values of air temperature $T = 273.0$ K, water vapor partial pressure $e = 1.43$ hPa, and carbon dioxide concentration $C = 380$ ppmv. (bottom) Dependence curve of $\beta(0.523~\mu\text{m})$ on air temperature $T$ for fixed values of parameters $p = 1013.0$ hPa, $e = 1.43$ hPa, and $C = 380$ ppmv.

**Table A1.** Arctic and Antarctic WMO Global Atmospheric Watch Stations, With Their Latitude, Longitude, and Altitude, and Yearly Average and Monthly Mean January and July Values of Carbon Dioxide Volume Concentration $C$ Measured at the Ground in 2007

| WDCGG Station[a] | Latitude | Longitude | Altitude (m above MSL) | Ground-Level $CO_2$ Volume Concentration $C$ (ppmv) | | |
|---|---|---|---|---|---|---|
| | | | | Yearly Average | Jan Average | Jul Average |
| Arctic stations | | | | | | |
| Ocean Station "M" | 66°00′N | 2°00′E | 7 | 384.1 ± 5.6 | 387.7 | 378.2 |
| Ny-Ålesund | 78°54′N | 11°53′E | 475 | 384.3 ± 6.0 | 388.2 | 378.8 |
| Pallas | 67°58′N | 24°07′E | 565 | 385.8 ± 6.9 | 390.2 | 376.5 |
| Teriberka | 69°12′N | 35°06′E | 40 | 384.6 ± 6.7 | 389.9 | 378.9 |
| Barrow | 71°19′N | 156°35′W | 11 | 384.9 ± 5.9 | 389.6 | 378.5 |
| Alert (NOAA/GMD) | 82°27′N | 62°31′W | 210 | 384.7 ± 6.0 | 388.8 | 380.0 |
| (CSIRO) | | | | 384.6 ± 6.0 | 388.7 | 380.4 |
| Summit | 72°35′N | 38°29′W | 3238 | 384.0 ± 4.7 | 386.9 | 379.4 |
| Antarctic stations | | | | | | |
| Palmer | 64°55′S | 64°00′W | 10 | 380.7 ± 1.1 | 379.0 | 381.0 |
| Halley Bay | 75°34′S | 26°30′W | 33 | 380.7 ± 1.0 | 379.3 | 380.9 |
| Syowa (NOAA/GMD, NIPR) | 69°00′S | 39°35′E | 29 | 380.8 ± 1.0 | 379.4 | 381.0 |
| Mawson | 67°37′S | 62°52′E | 32 | 380.3 ± 0.9 | 379.4 | 381.0 |
| South Pole (NOAA/GMD) | 89°59′S | 24°48′W | 2810 | 380.7 ± 1.0 | 379.6 | 380.9 |
| (CSIRO) | | | | 380.7 ± 1.0 | 379.6 | 380.8 |

[a]WDCGG denotes World Data Centre for Greenhoue Gases.

## References

Aaltonen, V., H. Lihavainen, M. Ginzburg, M. Kulmala, and Y. Viisanen (2006), Aerosol optical depth measurements in Finland and Antarctica in 2004–2006, in *Proceedings of BACCI, NECC and FCoE Activities 2005*, *Rep. Ser. Aerosol Sci.*, vol. 81A, edited by M. Kulmala, A. Lindroth, and T. M. Ruuskanen, pp. 30–32, Finn. Assoc. for Aerosol Res., Helsinki.

Adriani, A., P. Massoli, G. Di Donfrancesco, F. Cairo, M. L. Moriconi, and M. Snels (2004), Climatology of polar stratospheric clouds based on lidar observations from 1993 to 2001 over McMurdo Station, Antarctica, *J. Geophys. Res.*, *109*, D24211, doi:10.1029/2004JD004800.

Anderson, G. P., S. A. Clough, F. X. Kneizys, J. H. Chetwynd, and E. P. Shettle (1986), AFGL Atmospheric Constituent Profiles (0–120 km), *Environ. Res. Pap. 954*, Opt. Phys. Div., Air Force Geophys. Lab., Hanscom Air Force Base, Mass.

Ångström, A. (1964), The parameters of atmospheric turbidity, *Tellus*, *16*, 64–75.

Aoki, K., and Y. Fujiyoshi (2003), Sky radiometer measurements of aerosol optical properties over Sapporo, Japan, *J. Meteorol. Soc. Jpn*, *81*, 493–513.

Bates, D. R. (1984), Rayleigh scattering by air, *Planet. Space Sci.*, *32*, 785–790.

Beyerle, G., R. Neuber, O. Schrems, F. Wittrock, and B. Knudsen (1994), Multiwavelength lidar measurements of stratospheric aerosols above Spitsbergen during winter 1992/93, *Geophys. Res. Lett.*, *21*, 57–60.

Bideau–Mehu, A., Y. Guern, R. Abjean, and A. Johannin-Gilles (1973), Interferometric determination of the refractive index of carbon dioxide in the ultraviolet region, *Opt. Commun.*, *9*, 432–434.

Bigg, E. K. (1980), Comparison of aerosol at four baseline atmospheric monitoring stations, *J. Appl. Meteorol.*, *19*, 521–533.

Bodhaine, B. A. (1996), Central Antarctica: Atmospheric chemical composition and atmospheric transport, in *Chemical Exchange Between the Atmosphere and Polar Snow*, *NATO ASI Ser. I*, vol. 43, edited by E. W. Wolff and R. C. Bales, pp. 145–172, Springer, Berlin.

Bodhaine, B. A., and E. G. Dutton (1993), A long-term decrease in arctic haze at Barrow, Alaska, *Geophys. Res. Lett.*, *20*, 947–950.

Bodhaine, B. A., N. B. Wood, E. G. Dutton, and J. R. Slusser (1999), On Rayleigh optical depth calculations, *J. Atmos. Oceanic Technol.*, *16*, 1854–1861.

Bréon, F.-M. (1998), Comment on Rayleigh-scattering calculations for the terrestrial atmosphere, *Appl. Opt.*, *37*, 428–429.

Browell, E. V. (1991), Airborne lidar measurements of ozone and aerosols in the summertime Arctic troposphere, *Proc. SPIE Int. Soc. Opt. Eng.*, *1491*, 7–14, doi:10.1117/12.46641.

Bucholtz, A. (1995), Rayleigh-scattering calculations for the terrestrial atmosphere, *Appl. Opt.*, *34*, 2765–2773.

Cacciani, M., G. Fiocco, P. Colagrande, P. Di Girolamo, A. di Sarra, and D. Fuà (1997), Lidar observations of polar stratospheric clouds at the South Pole: 1. Stratospheric unperturbed conditions, 1990, *J. Geophys. Res.*, *102*, 12,937–12,943.

Cacciari, A., C. Tomasi, A. Lupi, V. Vitale, and S. Marani (2000), Radiative forcing effects by aerosol particles in Antarctica, *SIF Conf. Proc.*, *69*, 455–467.

Cairo, F., G. Di Donfrancesco, A. Adriani, L. Pulvirenti, and F. Fierli (1999), Comparison of various linear depolarization parameters measured by lidar, *Appl. Opt.*, *38*, 4425–4432.

Chiou, E.-W., M. P. McCormick, and W. P. Chu (1997), Global water vapor distributions in the stratosphere and upper troposphere derived from 5.5 years of SAGE II observations (1986–1991), *J. Geophys. Res.*, *102*, 19,105–19,118.

Ciddor, P. E. (1996), Refractive index of air: new equations for the visible and near infrared, *Appl. Opt.*, *35*, 1566–1573.

Ciddor, P. E. (2002), Refractive index of air: 3. The roles of $CO_2$, $H_2O$ and refractivity virials, *Appl. Opt.*, *41*, 2292–2298.

Dalgarno, A., and A. E. Kingston (1960), Refractive indices and Verdent constants of the inert gases, *Proc. R. Soc. A*, *259*, 424–429.

Damoah, R., N. Spichtinger, C. Forster, P. James, I. Mattis, U. Wandinger, S. Beirle, T. Wagner, and A. Stohl (2004), Around the world in 17 days—Hemispheric-scale transport of forest fire smoke from Russia in May 2003, *Atmos. Chem. Phys.*, *4*, 1311–1321.

Del Guasta, M., M. Morandi, L. Stefanutti, J. Brechet, and J. Piquad (1993), One year of cloud lidar data from Dumont d'Urville (Antarctica): 1. General overview of geometrical and optical properties, *J. Geophys. Res.*, *98*, 18,575–18,587.

de Mora, S. J., D. J. Wylie, and A. L. Dick (1997), Methanesulphonate and non-sea salt sulphate in aerosol, snow, and ice on the East Antarctic plateau, *Antarct. Sci.*, *9*, 46–55.

De Santis, L. V., C. Tomasi, and V. Vitale (1994), Characterization of Ångström's turbidity parameters in the Po Valley area for summer conditions of the atmosphere. Part II, *Nuovo Cimento C*, *17*, 407–430.

Di Carmine, C., M. Campanelli, T. Nakajima, C. Tomasi, and V. Vitale (2005), Retrievals of Antarctic aerosol characteristics using a Sun-sky radiometer during the 2001–2002 austral summer campaign, *J. Geophys. Res.*, *110*, D13202, doi:10.1029/2004JD005280.

Di Donfrancesco, G., A. Adriani, G. P. Gobbi, and F. Congeduti (1996), Lidar observations of stratospheric temperature above McMurdo Station, Antarctica, *J. Atmos. Sol. Terr. Phys.*, *58*, 1391–1399.

Donovan, D. P., A. I. Carswell, T. Shibata, J. C. Bird, T. J. Duck, T. Itabe, T. Nagai, S. R. Pal, O. Uchino, and J. A. Whiteway (1998), Multi-

wavelength lidar aerosol measurements made at Eureka (80°N, 86°W) during early 1995, *Geophys. Res. Lett.*, *25*, 3139–3142.

Dutton, E. G., and J. R. Christy (1992), Solar radiative forcing at selected locations and evidence for global lower tropospheric cooling following the eruptions of El Chichon and Pinatubo, *Geophys. Res. Lett.*, *19*, 2313–2316.

Edlén, B. (1966), The refractive index of air, *Metrologia*, *2*, 71–80.

Fiocco, G., M. Cacciani, A. di Sarra, D. Fuà, P. Colagrande, G. De Benedetti, and R. Viola (1996), The evolution of the Pinatubo stratospheric aerosol layer observed by lidar at South Pole, Rome, Thule: A summary of results, in *The Mount Pinatubo Eruption: Effects on the Atmosphere and Climate*, NATO/ASI Ser. I, vol. 42, edited by G. Fiocco, D. Fuà, and G. Visconti, pp. 17–32, Springer, Berlin.

Forster, C., et al. (2001), Transport of boreal forest fire emissions from Canada to Europe, *J. Geophys. Res.*, *106*, 22,887–22,906.

Harries, J. E., J. M. Russell III, A. F. Tuck, L. L. Gordley, P. Purcell, K. Stone, R. M. Bevilacqua, M. Gunson, G. Nedoluha, and W. A. Traub (1996), Validation of measurements of water vapor from the Halogen Occultation Experiment (HALOE), *J. Geophys. Res.*, *101*, 10,205–10,216.

Herber, A., L. W. Thomason, V. F. Radionov, and U. Leiterer (1993), Comparison of trends in the tropospheric and stratospheric aerosol optical depths in the Antarctic, *J. Geophys. Res.*, *98*, 18,441–18,447.

Herber, A., L. W. Thomason, K. Dethloff, P. Viterbo, V. F. Radionov, and U. Leiterer (1996), Volcanic perturbation of the atmosphere in both polar regions: 1991–1994, *J. Geophys. Res.*, *101*, 3921–3928.

Herber, A., L. W. Thomason, H. Gernandt, U. Leiterer, D. Nagel, K.-H. Schulz, J. Kaptur, T. Albrecht, and J. Notholt (2002), Continuous day and night aerosol optical depth observations in the Arctic between 1991 and 1999, *J. Geophys. Res.*, *107*(D10), 4097, doi:10.1029/2001JD000536.

Hogan, A. W., S. Barnard, and J. Bortiniak (1979), Physical properties of the aerosol at the South Pole, *Geophys. Res. Lett.*, *6*, 845–848.

Holben, B. N., et al. (1998), AERONET—A federated instrument network and data archive for aerosol characterization, *Remote Sens. Environ.*, *66*(1), 1–16.

Kawahara, T. D., T. Kitahara, F. Kobayashi, Y. Saito, A. Nomura, C.-Y. She, D. A. Krueger, and M. Tsutsumi (2002), Wintertime mesopause temperatures observed by lidar measurements over Syowa station (69°S, 39°E), Antarctica, *Geophys. Res. Lett.*, *29*(15), 1709, doi:10.1029/2002GL015244.

King, L. V. (1923), On the complex anisotropic molecule in relation to the dispersion and scattering of light, *Proc. R. Soc. A*, *104*, 333–357.

Klekociuk, A. R., M. M. Lambert, R. A. Vincent, and A. J. Dowdy (2003), First year of Rayleigh lidar measurements of middle atmosphere temperatures above Davis, Antarctica, *Adv. Space Res.*, *32*, 771–776.

Klett, J. D. (1985), Lidar inversion with variable backscatter/extinction ratio, *Appl. Opt.*, *24*, 1639–1643.

Lahoz, W. A., A. O'Neill, A. Heaps, V. D. Pope, R. Swinbank, R. S. Harwood, L. Froidevaux, W. G. Read, J. W. Waters, and G. E. Peckham (1996), Vortex dynamics and the evolution of water vapour in the stratosphere of the Southern Hemisphere, *Q. J. R. Meteorol. Soc.*, *122*, 423–450.

Larsen, N., B. Knudsen, T. S. Jorgensen, A. di Sarra, D. Fuà, P. Di Girolamo, G. Fiocco, M. Cacciani, J. M. Rosen, and N. T. Kjome (1994), Backscatter measurements of stratospheric aerosols at Thule during January–February 1992, *Geophys. Res. Lett.*, *21*, 1303–1306.

Luers, J. K. (1997), Temperature error of the Vaisala RS90 radiosonde, *J. Atmos. Oceanic Technol.*, *14*, 520–1532.

Luers, J. K., and R. E. Eskridge (1995), Temperature corrections for the VIZ and Vaisala radiosondes, *J. Appl. Meteorol.*, *34*, 1241–1253.

Mahesh, A., J. R. Campbell, and J. D. Spinhirne (2005), Multi-year measurements of cloud base heights at South Pole by lidar, *Geophys. Res. Lett.*, *32*, L09812, doi:10.1029/2004GL021983.

Miloshevich, L. M., A. Paukkunen, H. Vömel, and S. J. Oltmans (2004), Development and validation of a time-lag correction for Vaisala radiosonde humidity measurements, *J. Atmos. Oceanic Technol.*, *21*, 1305–1327.

Miloshevich, L. M., H. Vömel, D. N. Whiteman, B. M. Lesht, F. J. Schmidlin, and F. Russo (2006), Absolute accuracy of water vapour measurements from six operational radiosonde types launched during AWEX-G and implications for AIRS validation, *J. Geophys. Res.*, *111*, D09S10, doi:10.1029/2005JD006083.

Minikin, A., M. Legrand, J. Hall, D. Wagenbach, C. Kleefeld, E. Wolff, E. C. Pasteur, and F. Ducroz (1998), Sulfur-containing species (sulfate and MSA) in coastal Antarctic aerosol and precipitation, *Geophys. Res.*, *103*, 10,975–10,990.

Morrey, M. W., and R. S. Harwood (1998), Interhemispheric differences in stratospheric water vapour during late winter, in version 4 MLS measurements, *Geophys. Res. Lett.*, *25*, 147–150.

Müller, M., R. Neuber, F. Fierli, A. Hauchecorne, H. Vömel, and S. J. Oltmans (2003a), Stratospheric water vapour as tracer for vortex filamentation in the Arctic winter 2002/2003, *Atmos. Chem. Phys. Discuss.*, *3*, 4393–4410.

Müller, M., R. Neuber, and S. Fueglistaler (2003b), Winter 2002/2003: PSC observations by lidar in Ny-Ålesund, Spitsbergen, *Geophys. Res. Abstr.*, *5*, 01915.

Myhre, C. L., K. Stebel, C. Toledano, V. E. Cachorro, A. M. de Frutos, C. Forster, and J. Schaug (2006), Aerosol optical depth in the European Arctic Region, in *EMEP/CCC-Report 3/2006, Measurements of Particulate Matter: Status Report 2006*, chap. 5, pp. 73–80, Norw. Inst. for Air Res., Kjeller, Norway.

Nagel, D., A. Herber, L. W. Thomason, and U. Leiterer (1998), Vertical distribution of the spectral aerosol optical depth in the Arctic from 1993 to 1996, *J. Geophys. Res.*, *103*, 1857–1870.

Owens, J. C. (1967), Optical refractive index of air: Dependence on pressure, temperature and composition, *Appl. Opt.*, *6*, 51–59.

Pan, W., C. S. Gardner, and R. G. Roble (2002), The temperature structure of the winter atmosphere at South Pole, *Geophys. Res. Lett.*, *29*(16), 1802, doi:10.1029/2002GL015288.

Peck, R., and K. Reeder (1972), Dispersion of air, *J. Opt. Soc. Am.*, *62*, 958–962.

Penndorf, R. (1957), Tables of the refractive index for standard air and the Rayleigh scattering coefficient for the spectral region between 0.2 and 20.0 $\mu$m and their application to atmospheric optics, *J. Opt. Soc. Am.*, *47*, 176–182.

Peter, R. (1998), Stratospheric and mesospheric latitudinal water vapour distributions obtained by an airborne millimeter-wave spectrometer, *J. Geophys. Res.*, *103*, 16,275–16,290.

Petkov, B., V. Vitale, C. Tomasi, U. Bonafè, S. Scaglione, D. Flori, R. Santaguida, M. Gausa, G. Hansen, and T. Colombo (2006), Narrowband filter radiometer for ground-based measurements of global ultraviolet solar irradiance and total ozone, *Appl. Opt.*, *45*, 4383–4395.

Piel, C., R. Weller, M. Huke, and D. Wagenbach (2006), Atmospheric methane sulfonate and non-sea-salt sulfate records at the European Project for Ice Coring in Antarctica (EPICA) deep-drilling site in Dronning Maud Land, Antarctica, *J. Geophys. Res.*, *111*, D03304, doi:10.1029/2005JD006213.

Ponczkowska, A., T. Zielinski, T. Petelski, K. Markowicz, G. Chourdakis, and G. Georgoussis (2009), Aerosol optical depth measured at different coastal boundary layers and its links with synoptic-scale features, *Remote Sens.*, *1*, 557–576, doi:10.3390/rs1030557.

Quinn, P. K., T. L. Miller, T. S. Bates, J. A. Ogren, E. Andrews, and G. E. Shaw (2002), A 3-year record of simultaneously measured aerosol chemical and optical properties at Barrow, Alaska, *J. Geophys. Res.*, *107*(D11), 4130, doi:10.1029/2001JD001248.

Radionov, V. F. (1994), Variability of aerosol extinction of solar radiation in Antarctica, *Antarct. Sci.*, *6*, 419–424.

Radionov, V. F. (2005), Temporal variability of the aerosol optical characteristics of the atmosphere in the Russian Arctic (historical review), in *WMO/GAW Experts Workshop on a Global Surface Based Network for Long Term Observations of Column Aerosol Optical Properties, WMO TD 1287*, pp. 82–85, World Meteorol. Org., Geneva.

Radionov, V. F., and M. S. Marshunova (1992), Long-term variations in the turbidity of the Arctic atmosphere in Russia, *Atmos. Ocean*, *30*(4), 531–549.

Radionov, V. F., M. S. Marshunova, E. N. Rusina, K. E. Lubo-Lesnichenko, and Y. E. Pimanova (1994), Atmospheric aerosol turbidity over polar regions, *Izv. Atmos. Ocean Phys.*, *30*, 797–801.

Radionov, V. F., M. V. Lamakin, and A. Herber (2002), Changes in the aerosol optical depth of the Antarctic atmosphere, *Izv. Atmos. Ocean Phys.*, *38*, 205–210.

Randel, W. J., F. Wu, A. Gettelman, J. M. Russell III, J. M. Zawodny, and S. J. Oltmans (2001), Seasonal variation of water vapor in the lower stratosphere observed in Halogen Occultation Experiment data, *J. Geophys. Res.*, *106*, 14,313–14,325.

Rind, D., E.-W. Chiou, W. Chu, S. Oltmans, J. Lerner, J. Larsen, M. P. McCormick, and L. McMaster (1993), Overview of the Stratospheric Aerosol and Gas Experiment II water vapor observations: Method, validation, and data characteristics, *J. Geophys. Res.*, *98*, 4835–4856.

Rosen, J. M., N. T. Kjome, and S. J. Oltmans (1991), Balloon borne observations of backscatter, frost point and ozone in polar stratospheric clouds at South Pole, *Geophys. Res. Lett.*, *18*, 171–174.

Russell, J. M., III, J. C. Gille, E. E. Remsberg, L. L. Gordley, P. L. Bailey, H. Fischer, A. Girard, S. R. Drayson, W. F. J. Evans, and J. E. Harries (1984), Validation of water vapor results measured by the Limb Infrared Monitor of the Stratosphere Experiment on NIMBUS 7, *J. Geophys. Res.*, *89*, 5115–5124.

Scateboe, R. (1996), ALOMAR: Atmospheric science using lidars, radars, and ground based instruments, *J. Atmos. Sol. Terr. Phys.*, *58*, 1823–1826.

Sharma, S., E. Andrews, L. A. Barrie, J. A. Ogren, and D. Lavoué (2006), Variations and sources of equivalent black carbon in the high Arctic revealed by long-term observations at Alert and Barrow: 1989–2003, *J. Geophys. Res.*, *111*, D14208, doi:10.1029/2005JD006581.

Shaw, G. E. (1976), Error analysis of multi-wavelength Sun photometry, *Pure Appl. Geophys.*, *114*, 1–14.

Shaw, G. E. (1982), Atmospheric turbidity in the polar regions, *J. Appl. Meteorol.*, *21*, 1080–1088.

Shaw, G. E. (1983), Evidence of a central Eurasian source area of Arctic haze in Alaska, *Nature*, *299*, 815–818.

Shaw, G. E. (1988), Antarctic aerosols: A review, *Rev. Geophys.*, *26*, 89–112.

Six, D., M. Fily, L. Blarel, and P. Goloub (2005), First aerosol optical thickness measurements at Dome C (East Antarctica), summer season 2003–2004, *Atmos. Environ.*, *39*, 5041–5050.

Solomon, S., A. Schmeltekopf, and R. W. Sanders (1987), On the interpretation of zenith sky absorption measurements, *J. Geophys. Res.*, *92*, 8311–8319.

Stohl, A., B. Andrews, J. F. Burkhart, C. Forster, D. Kowal, C. Lunder, T. Mefford, J. A. Ogren, S. Sharma, N. Spichtinger, K. Stebel, R. Stone, J. Ström, and K. Tørseth (2006), Pan-Arctic enhancements of light absorbing aerosol concentrations due to North American boreal forest fires during summer 2004, *J. Geophys. Res.*, *111*, D22214, doi:10.1029/2006JD007216.

Stone, R. S. (2002), Monitoring aerosol optical depth at Barrow, Alaska, and South Pole; Historical overview, recent results and future goals, *SIF Conf. Proc.*, *80*, 123–144.

Stone, R. S., J. Key, and E. Dutton (1993), Properties and decay of stratospheric aerosols in the Arctic following the 1991 eruptions of Mount Pinatubo, *Geophys. Res. Lett.*, *20*, 2359–2362.

Stone, R., G. Anderson, E. Andrews, E. Dutton, J. Harris, E. Shettle, and A. Berk (2005), Asian dust signatures at Barrow: Observed and simulated incursions and impact of Asian dust over Northern Alaska, paper presented at Workshop on Remote Sensing of Atmospheric Aerosol, An Honorary Workshop for Professor J. A. Reagan, Inst. of Electr. and Electron. Eng., Tucson, Ariz.

Ström, J., J. Umegård, K. Tørseth, P. Tunved, H.-C. Hansson, K. Holmén, V. Wismann, A. Herber, and G. König-Langlo (2003), One year of particle size distribution and aerosol chemical composition measurements at the Zeppelin station, Svalbard, March 2000–March 2001, *Phys. Chem. Earth*, *28*, 1181–1190.

Tanaka, M., T. Nakajima, and M. Shiobara (1986), Calibration of a Sun photometer by simultaneous measurements of direct-solar and circumsolar radiations, *Appl. Opt.*, *25*, 1170–1176.

Teinilä, K., V.-M. Kerminen, and R. Hillamo (2000), A study of size-segregated aerosol chemistry in the Antarctic atmosphere, *J. Geophys. Res.*, *105*, 3893–3904.

Toledano, C., V. E. Cachorro, A. Berjón, M. Sorribas, R. Vergaz, Á. M. deFrutos, M. Antón, and M. Gausa (2006), Aerosol optical depth at ALOMAR Observatory (Andøya, Norway) in summer 2002 and 2003, *Tellus, Ser. B*, *58*, 218–228.

Tomasi, C., F. Prodi, M. Sentimenti, and G. Cesari (1983), Multiwavelength Sun-photometers for accurate measurements of atmospheric extinction in the visible and near-IR spectral range, *Appl. Opt.*, *22*, 622–630.

Tomasi, C., V. Vitale, and M. Tagliazucca (1989), Atmospheric turbidity measurements at Terra Nova Bay during January and February 1988, *SIF Conf. Proc.*, *20*, 67–77.

Tomasi, C., V. Vitale, and G. Zibordi (1991), Multiwavelength sun-photometric measurements of the atmospheric turbidity parameters at Terra Nova Bay during January 1990, *SIF Conf. Proc.*, *34*, 125–142.

Tomasi, C., S. Marani, V. Vitale, F. Wagner, A. Cacciari, and A. Lupi (2000), Precipitable water evaluations from infrared Sun-photometric measurements analyzed using the atmospheric hygrometry technique, *Tellus, Ser. B*, *52*, 734–749.

Tomasi, C., A. Cacciari, V. Vitale, A. Lupi, C. Lanconelli, A. Pellegrini, and P. Grigioni (2004), Mean vertical profiles of temperature and absolute humidity from a twelve-year radiosounding data-set at Terra Nova Bay (Antarctica), *Atmos. Res.*, *71*, 139–169.

Tomasi, C., V. Vitale, B. Petkov, A. Lupi, and A. Cacciari (2005), Improved algorithm for calculations of Rayleigh-scattering optical depth in standard atmospheres, *Appl. Opt.*, *44*, 3320–3341.

Tomasi, C., et al. (2006), Characterization of the atmospheric temperature and moisture conditions above Dome C (Antarctica) during austral summer and fall months, *J. Geophys. Res.*, *111*, D20305, doi:10.1029/2005JD006976.

Tomasi, C., et al. (2007), Aerosols in polar regions: A historical overview based on optical depth and in situ observations, *J. Geophys. Res.*, *112*, D16205, doi:10.1029/2007JD008432.

Turner, D. D., B. M. Lesht, S. A. Clough, J. C. Liljegren, H. E. Revercomb, and D. C. Tobin (2003), Dry bias and variability in Vaisala RS80-H radiosondes: The ARM experience, *J. Atmos. Oceanic Technol.*, *20*, 117–132.

Virkkula, A., I. K. Koponen, R. Hillamo, and M. Kulmala (2000), Optical properties and volume concentration of atmospheric aerosol between Europe and Antarctica, *J. Aerosol Sci.*, *31*, S272–S273.

Vitale, V., and V. F. Radionov (2005), Aerosol optical depth measurements in polar regions, in *WMO/GAW Experts Workshop on a Global Surface Based Network for Long Term Observations of Column Aerosol Optical Properties*, *WMO TD 1287*, pp. 75–81, World Meteorol. Org., Geneva.

Vitale, V., and C. Tomasi (1990), Atmospheric turbidity measurements at Terra Nova Bay with the multispectral Sun-photometer model UVISIR, *SIF Conf. Proc.*, *27*, 89–104.

von Hoyningen-Huene, W., M. Freitag, and J. P. Burrows (2003), Retrieval of aerosol optical thickness over land surfaces from top-of-atmosphere radiance, *J. Geophys. Res.*, *108*(D9), 4260, doi:10.1029/2001JD002018.

Wang, J., H. L. Cole, D. J. Carlson, E. R. Miller, K. Beierle, A. Paukkunen, and T. K. Laine (2002), Corrections of humidity measurement errors from the Vaisala RS80 radiosonde—Application to TOGA COARE data, *J. Atmos. Oceanic Technol.*, *19*, 981–1002.

Wehrli, C. (2005), GAWPFR: A network of aerosol optical depth observations with precision filter radiometers in *WMO/GAW Experts Workshop on a Global Surface based Network for Long Term Observations of Column Aerosol Optical Properties*, *WMO TD 1287*, pp. 36–39, World Meteorol. Org., Geneva.

Wolff, E. W., and H. Cachier (1998), Concentrations and seasonal cycle of black carbon in aerosol at a coastal Antarctic station, *J. Geophys. Res.*, *103*, 11,033–11,041.

Young, A. T. (1980), Revised depolarization corrections for atmospheric extinction, *Appl. Opt.*, *19*, 3427–3428.

_____

E. Benedetti, ICES Group, Institute of Acoustic "O.M. Corbino," Consiglio Nazionale delle Ricerche, via Fosso del Cavaliere 100, I-00133 Rome, Italy.

A. Herber, Climate System Division, Alfred Wegener Institute for Polar and Marine Research, Am Handelshafen 12, D-27570 Bremerhaven, Germany.

C. Lanconelli, A. Lupi, M. Mazzola, B. Petkov, C. Tomasi, and V. Vitale, Institute of Atmospheric Sciences and Climate (ISAC), Consiglio Nazionale delle Ricerche (CNR), via Gobetti 101, I-40129, Bologna, Italy. (c.tomasi@isac.cnr.it)

R. S. Stone, Cooperative Institute for Research in Environmental Sciences, University of Colorado, Boulder, Colorado 80305, USA.

W. von Hoyningen-Huene, Remote Sensing, Institute of Environmental Physics, University of Bremen, Kufsteiner Strasse NW1, D-28359 Bremen, Germany.